symmetry

IMPACT FACTOR 2.940

CITESCORE 4.3

Article

The Role of the Hidden Color Channel in Some Interesting Dibaryon Candidates

Lianrong Dai, Yuhang Wang, Langning Chen and Tiange Zhang

Special Issue

Symmetry in Nuclear Physics: Model Calculations, Advances and Applications

Edited by

Prof. Dr. Jerry Paul Draayer, Dr. Feng Pan and Dr. Andriana Martinou

MDPI

https://doi.org/10.3390/sym15020446

symmetry

MDPI

Article

The Role of the Hidden Color Channel in Some Interesting Dibaryon Candidates

Lianrong Dai [1,2,*], Yuhang Wang [2], Langning Chen [2] and Tiange Zhang [2]

[1] School of Science, Huzhou University, Huzhou 313000, China
[2] Department of Physics, Liaoning Normal University, Dalian 116029, China
* Correspondence: dailianrong@zjhu.edu.cn

Abstract: Nowadays, exploring dibaryon candidates has attracted much attention, both theoretically and experimentally. It is important to find a reasonable model to predict the possible dibaryon candidates. The chiral SU(3) quark model is just one of the most successful models, with which we can reasonably explain the experimental binding energies of baryon's ground state and the properties of deuteron, NN and YN scattering processes. By utilizing the same set of model parameters, we predicted the nonstrange d^* dibaryon with a binding energy of 84 MeV, which is consistent with a recent experiment in which we also found that the hidden color (CC) channel plays an important role in forming this bound state. Due to the theoretical investigation of the CC channel being scarce for dibaryons, we explore other possible and interesting dibaryon candidates in the present work. According to the symmetry properties, we chose six interesting candidates, including strangeness $0, -1, -5, -6$ systems. All the hidden color wave functions were built, and the spin-flavor-color matrix elements were systematically evaluated. Then, we applied these obtained matrix elements to further dynamically solve the corresponding resonating group method's equation in a coupled-channel calculation. The results show that the coupling to the CC channel plays an significant role in forming each spin S = 3 state, where tensor coupling is also included and has an obvious effect in forming each S = 0 state. The present work is significant in helping us to acquire deeper understanding of the effects of the hidden color channel and QCD phenomenology.

Keywords: quark model; chiral Lagrangian; dibaryon; hidden color channel; resonating group method

Citation: Dai, L.; Wang, Y.; Chen, L.; Zhang, T. The Role of the Hidden Color Channel in Some Interesting Dibaryon Candidates. *Symmetry* **2023**, *15*, 446. https://doi.org/10.3390/sym15020446

Academic Editor: Jorge Segovia

Received: 18 December 2022
Revised: 28 January 2023
Accepted: 30 January 2023
Published: 7 February 2023

1. Introduction

The exciting story started in 2014, when the WASA-at-COSY collaboration found a peak in the $pn \to d\pi^0\pi^0$ fusion reaction that was associated with a d^* dibaryon [1], corresponding to a nonstrange $\Delta\Delta$ dibaryon, its spin $S = 3$ and isospin $T = 0$. The binding energy is 84 MeV, indicating a deeply bound state. Since then, the exploration of other possible dibaryon states has again attracted extensive attention both theoretically and experimentally [2–15]. As is well known, the first and the most famous state is the deuteron, which was discovered in 1932 [16]. It is composed of a proton–neutron system (pn) with $S = 1$ and $T = 0$. The deuteron is a loosely bound state with a binding energy of only 2.2 MeV. After that, no any other possible dibaryons were ever found in experiments for many years till 2014 [1].

Dibaryon is an important way to study the non-perturbative effect of quantum chromodynamics (QCD), which is the underlying theory of the strong interaction. Back in 1964, firstly, Gell–Mann proposed the existence of dibaryons [17]. Since then, many predictions on the existence of possible dibaryon candidates have been found. Triggered by the prediction of the H dibaryon [18], many other predictions later appeared: the potential model, bag model and string and flux tube models for the dibaryon systems [19–38].

Before 2014, there were actually many theoretical investigations on nonstrange d^* structure [32–39]; the predicted binding energies ranged from about 10 to 390 MeV. Among

these models, it should be noted that the predictions in [38,39] are fairly consistent with the experiments [1], in which the chiral and extended SU(3) quark models were utilized, and importantly, the effect of the hidden-color channel (CC) is under consideration. We found that the CC channel plays an important role in the binding behavior of the d^* system.

After 2014, there were also many theoretical studies on the properties of the d^* state, reporting it as a compact hexaquark, such as the extended Gürsey–Radicati model [40], the QCD sum rules [41], Lattice QCD [11], the quark delocalization color screening model [42] and the chiral SU(3) quark model [43–45].

The extended chiral SU(3) quark model [46] was proposed based on the chiral SU(3) quark model [47]. This model is one of the most successful QCD-inspired models. We can reasonably explain the binding energies of baryon ground states, the properties of deuteron, the nucleon–nucleon (NN) and hyperon–nucleon (YN) scattering processes by dynamically solving the resonating group method (RGM) equation. When extending this model to d^* investigations, no additional parameters are required, and surprisingly, we found that our predictions are in good agreement with an experiment [1].

Naturally, we would like to extend to some other possible and interesting dibaryon candidates with different strangeness, further exploring the effects from different CC channels.

Here, we would like to add some remarks on our proposed chiral SU(3) and extended chiral SU(3) quark models [46,47]. The above two models have been proposed based on the two pioneering works where the quark model made its great leap of being able to describe NN scattering data based on quark degrees of freedom [48,49]. It was the first time that the one sigma exchange was considered at the quark level, and hadronic potentials were not used at long range due to the mentioned pioneer works. Therefore, the exchange mechanism from sigma meson is important in our chiral quark models [46,47].

As we know, a baryon is composed of three quarks in a quark model, and it is described by a fully antisymmetric wave function including the spatial degree and the internal degrees of freedom, which contain flavor, spin and color parts. The flavor degree of freedom is taken to be the three light flavors of u, d and s. The spin degree of freedom is taken to be the two spin components $\uparrow, \downarrow$. The color degree of freedom is taken to be the three colors of r, g and b.

Let us come back to the question of the dibaryon. In a summary work of dibaryon [31], the authors performed an analysis telling us that two major factors will affect the binding behavior. The first is the symmetry property, and the second is the interactions between quarks, especially the quark chiral field-induced interactions. They used the following matrix element to characterize the symmetry property:

$$\langle \mathcal{A}^{\mathrm{sfc}} \rangle = \langle 1 - \sum_{i=1}^{3} \sum_{j=4}^{6} P_{ij}^{\mathrm{sfc}} \rangle = \langle 1 - 9 P_{36}^{\mathrm{sfc}} \rangle$$

where quarks 1, 2 and 3 are inside cluster A; quarks 4, 5 and 6 are inside cluster B; and sfc denotes the operator that acts within the spin-flavor-color space; thus, P_{36}^{sfc} denotes how the permutation operator acts in sfc space, and 36 represents the exchange operation between the 3rd and 6th quarks of cluster $A(123)$ and $B(456)$, respectively. For the baryon-baryon state, the $\langle \mathcal{A}^{\mathrm{sfc}} \rangle$ is important to measure the action of the Pauli principle. It is shown that six interesting candidates belong to $\langle \mathcal{A}^{\mathrm{sfc}} \rangle = 2$. These systems would be enormously beneficial to form a state due to highly symmetric character of $[6]_{\mathrm{O}}$ in orbital space. This is exactly the reason why we decided to study these six dibaryon candidates in the present work.

We have mentioned above that in our works of [38,39], the predictions of d^* structure are very consistent with the recent experiment. This finding is surprising, and more importantly, the CC channel was found to play an important role in this system. It is of interest to investigate the effect from CC channel on different systems. An earlier discussion can be found in [50,51], and a later one in [52–55], based on group theory. In refs. [50,51], the author constructed the CC state by using the expansion coefficients of fractional parentage (cfp) method. Based upon this work, Zongye Zhang derived the relation of symmetry basis

and physical basis for the $\Delta\Delta$ system, in which she found a new method to construct the CC state. In her method, the complicated calculations in group theory can be avoided, and she constructed the CC wave function and further computed all the sfc matrix elements. Then, these sfc matrix elements were firstly applied into the dynamical calculation for studying the d^* structure [38], where the sfc matrix elements are also tabulated. We can see that $\langle CC|\lambda_1^c \cdot \lambda_2^c|CC\rangle = -\frac{2}{3}$, which is consistent with the calculation in [50], verifying that the constructed CC wave function is correct.

As the theoretical investigation of CC channel on dibaryon system is scarce, in the present work we would like to develop the method proposed by Zongye Zhang for other interesting dibaryon candidates with different strangeness, further exploring the effect of CC channel in the binding behavior of the dibaryon. We systematically investigated the six interesting dibaryon candidates, showing the reader how to obtain the CC wave function and evaluate the needed sfc elements for each candidates. Finally, we performed the dynamical calculations in our chiral SU(3) quark model within the framework of the resonating group method.

The paper is arranged as follows: Firstly, we briefly introduce the chiral SU(3) quark model in Section 2, and then we discuss the calculated results in the single-channel case in Section 3, in which we also analyze the symmetry characters of the six systems. An extension to include the CC channel, how to construct the CC wave function and the obtained sfc matrix elements are presented in Section 4. Finally, we come to the concluding remarks in Section 5.

2. Formalism

2.1. The Chiral SU(3) Quark Model

Although QCD is believed to be the basis theory of the strong interaction, one has to develop some QCD-inspired models due to the complexity of the non-perturbative QCD at the lower energy region. Among these models, the constituent quark model (CQM) has been quite successful in dynamically studying the NN interaction [56–60]. The short-range repulsive feature can be explained by both the quark-exchange effect and the one-gluon-exchange (OGE) interaction in this model. However, the source of the constituent quark mass is not clear, and as long as the quark carries constituent mass (about several hundred MeV), the chiral symmetry of the Lagrangian, which is very important in hadron physics, is broken. Therefore, one should restore the chiral symmetry of the model, such as in the work of [48]. Actually we ever proposed another method to restore the chiral symmetry in the flavor SU(2) case [61]; then, we further generalized to the flavor SU(3) case, proposing the chiral SU(3) quark model [47]. In this model, by using the linear realization of the Lagrangian, we derive the quark–quark potential. This Lagrangian is proven invariant under the chiral transformation, and the interaction Lagrangian is written as

$$\mathcal{L}_{\rm I} = -g_{\rm ch}(\bar{\psi}_L \Sigma \psi_R - \bar{\psi}_R \Sigma^+ \psi_L)\,, \tag{1}$$

with ψ_L and ψ_R being the quark-left and right spinors, respectively, and $g_{\rm ch}$ being the quark-chiral field coupling constant. Generalizing the linear realization of Σ, one obtains

$$\mathcal{L}_{\rm I} = -g_{\rm ch}\bar{\psi}\left(i\sum_{a=0}^{8}\pi_a\lambda_a\gamma_5 + \sum_{a=0}^{8}\sigma_a\lambda_a\right)\psi\,, \tag{2}$$

where ψ is the quark field; π_a denotes the pseudoscalar nonet chiral fields π, K, η, η'; σ_a is the scalar nonet field; $\sigma', \kappa, \epsilon, \sigma$ and λ_a are the generators of the flavor SU(3) group. Consequently, the interactive Hamiltonian becomes

$$H_{\rm ch} = g_{ch}F(q^2)\bar{\psi}\left(+i\sum_{a=0}^{8}\pi_a\lambda_a\gamma_5 + \sum_{a=0}^{8}\sigma_a\lambda_a\right)\psi\,. \tag{3}$$

where we have inserted a form factor $F(q^2)$ to describe the chiral field's structure, which, as usual, is taken as

$$F(q^2) = \left(\frac{\Lambda^2}{\Lambda^2 + q^2}\right)^{1/2}, \tag{4}$$

where we use the cutoff mass Λ to indicate the chiral-symmetry-breaking scale.

Now, the total Hamiltonian can be written as

$$H = \sum_{i=1}^{6} T_i - T_G + \sum_{j>i=1}^{6} V_{ij}, \tag{5}$$

where T_i denotes the ith quark kinetic energy, T_G is kinetic energy of center of mass motion and

$$V_{ij} = V_{ij}^{\text{conf}} + V_{ij}^{\text{OGE}} + V_{ij}^{\text{ch}}. \tag{6}$$

It includes three parts: V_{ij}^{conf} is the confinement potential, which describes the long-distance effect; V_{ij}^{OGE} is one-gluon-exchange (OGE) potential, which describes the short-range effect; V_{ij}^{ch} is the quark chiral SU(3) field-induced interaction, including the pseudoscalar exchanges and the scalar exchanges between two quarks. The explicit expressions are listed below:

$$V_{ij}^{\text{conf}} = -\left(\lambda_i^c \cdot \lambda_j^c\right)\left(a_{ij}^c r_{ij}^2 - a_{ij}^{c0}\right) \tag{7}$$

$$V_{ij}^{\text{OGE}} = \frac{1}{4} g_i g_j (\lambda_i^c \cdot \lambda_j^c)\left\{\frac{1}{r_{ij}} - \frac{\pi}{2}\delta(\boldsymbol{r}_{ij})\left(\frac{1}{m_{q_i}^2} + \frac{1}{m_{q_j}^2} + \frac{4}{3}\frac{\boldsymbol{\sigma}_i \cdot \boldsymbol{\sigma}_j}{m_{q_i} m_{q_j}}\right) - \frac{1}{4 m_{q_i} m_{q_j} r_{ij}^3} S_{ij}\right\} \tag{8}$$

$$\begin{aligned}
V_{ij}^{\text{ch}} &= \sum_{a=0}^{8} V_{ij}^{\pi_a} + \sum_{a=0}^{8} V_{ij}^{\sigma_a}, \\
V_{ij}^{\sigma_a} &= -C(g_{\text{ch}}, m_{\sigma_a}, \Lambda)(\lambda_a(i)\lambda_a(j)) X_1(m_{\sigma_a}, \Lambda, r_{ij}), \\
V_{ij}^{\pi_a} &= C(g_{\text{ch}}, m_{\pi_a}, \Lambda)(\lambda_a(i)\lambda_a(j))\frac{m_{\pi_a}^2}{12 m_{q_i} m_{q_j}} \\
&\times \left\{X_2(m_{\pi_a}, \Lambda, r_{ij})(\boldsymbol{\sigma_i} \cdot \boldsymbol{\sigma_j}) + \left(H(m_{\pi_a} r_{ij}) - (\frac{\Lambda}{m_{\pi_a}})^3 H(\Lambda r_{ij})\right) S_{ij}\right\},
\end{aligned} \tag{9}$$

where m_q is the mass of quark and r_{ij} is the relative distance between two quarks, and

$$\begin{aligned}
S_{ij} &= 3(\boldsymbol{\sigma}_i \cdot \hat{\boldsymbol{r}})(\boldsymbol{\sigma}_j \cdot \hat{\boldsymbol{r}}) - (\boldsymbol{\sigma}_i \cdot \boldsymbol{\sigma}_j), \\
C(g_{\text{ch}}, m, \Lambda) &= \frac{g_{\text{ch}}^2}{4\pi}\frac{\Lambda^2}{\Lambda^2 - m^2} m, \\
X_1(m, \Lambda, r) &= Y(mr) - \frac{\Lambda}{m} Y(\Lambda r), \\
X_2(m, \Lambda, r) &= Y(mr) - \frac{\Lambda^3}{m^3} Y(\Lambda r), \\
Y(x) &= \frac{1}{x} e^{-x}, \quad H(x) = (1 + \frac{3}{x} + \frac{3}{x^2}) Y(x).
\end{aligned} \tag{10}$$

and more details can be found in ref. [47].

2.2. Baryon Octet

We use a totally antisymmetric wave function to describe a baryon octet with spin 1/2, including orbit (O), flavor (F), spin (S) and color (C) spaces, and it can be written using the Young tableaux method:

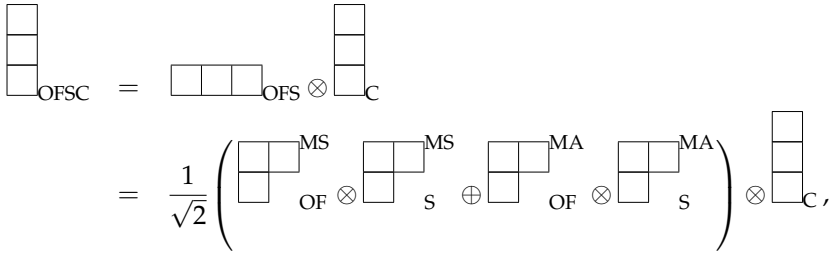

(11)

where the MS and MA label a mixed symmetric and a mixed antisymmetric state, respectively. The orbital flavor (OF) parts of wave function mean that the orbital part has a flavor index, which cannot be separated from the flavor part. The nucleon wave functions used in the calculation for deuteron in flavor and spin spaces are listed in Tables 1 and 2, respectively.

Table 1. The flavor wave function for nucleon.

$\|T, M_T\rangle$	$[21]_{\mathbf{F}}^{\mathbf{MS}}$	$[21]_{\mathbf{F}}^{\mathbf{MA}}$	**Octet**
$\|\frac{1}{2}, \frac{1}{2}\rangle$	$-\sqrt{\frac{1}{6}}\|udu + duu - 2uud\rangle$	$\sqrt{\frac{1}{2}}\|udu - duu\rangle$	p
$\|\frac{1}{2}, -\frac{1}{2}\rangle$	$\sqrt{\frac{1}{6}}\|udd + dud - 2ddu\rangle$	$\sqrt{\frac{1}{2}}\|udd - dud\rangle$	n

Table 2. The spin wave function for baryon with spin $S = \frac{1}{2}$.

$\|S, M_s\rangle$	$[21]_{\mathbf{S}}^{\mathbf{MS}}$	$[21]_{\mathbf{S}}^{\mathbf{MA}}$
$\|\frac{1}{2}, \frac{1}{2}\rangle$	$-\sqrt{\frac{1}{6}}\|\uparrow\downarrow\uparrow + \downarrow\uparrow\uparrow - 2\uparrow\uparrow\downarrow\rangle$	$\sqrt{\frac{1}{2}}\|\uparrow\downarrow\updownarrow - \downarrow\uparrow\uparrow\rangle$
$\|\frac{1}{2}, -\frac{1}{2}\rangle$	$\sqrt{\frac{1}{6}}\|\uparrow\downarrow\downarrow + \downarrow\uparrow\downarrow - 2\downarrow\downarrow\uparrow\rangle$	$\sqrt{\frac{1}{2}}\|\uparrow\downarrow\downarrow - \downarrow\uparrow\downarrow\rangle$

Baryon is considered as a color singlet with $|[111]\rangle_C$ symmetry in color space; thus, the color singlet can be written as

$$|[111]\rangle_C = \sqrt{\frac{1}{6}}|rgb + gbr + brg - rbg - grb - bgr\rangle\,. \tag{12}$$

We should stress that for an orbital flavor wave function of baryon octet A, the explicit expression is

$$\begin{aligned} |\mathrm{A}\rangle_{\mathrm{OF}[21]}^{\mathrm{MX}} &= \sum_{f_1 f_2 f_3} {}^{\mathrm{A}}C_{[21]}^{\mathrm{MX}}(f_1 f_2 f_3)\,|f_1 f_2 f_3\rangle_{\mathrm{OF}} \\ &= \sum_{f_1 f_2 f_3} {}^{\mathrm{A}}C_{[21]}^{\mathrm{MX}}(f_1 f_2 f_3)\,|f_1 f_2 f_3\rangle_{\mathrm{F}} \times \Phi_{3q}^{\mathrm{A}}(\boldsymbol{r}_1, f_1; \boldsymbol{r}_2, f_2; \boldsymbol{r}_3, f_3)\,, \end{aligned} \tag{13}$$

where the coefficients ${}^{\mathrm{A}}C_{[21]}^{\mathrm{MX}}(f_1 f_2 f_3)$ are the standard SU(3) Clebsch–Gordan coefficients, and MX denotes the MS or MA components [62].

2.3. Baryon Decuplet

We also used a totally antisymmetric wave function to describe a baryon decuplet state with spin 3/2 which can be written using the similar Young tableaux method:

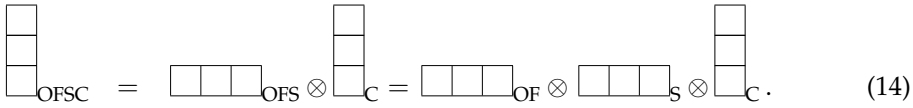

(14)

It is noted again that the orbit wave function will depend on the different quark masses; thus, it has a flavor index which cannot be separated from the flavor part.

$$\begin{aligned} |\mathrm{A}\rangle_{\mathrm{OF}[3]} &= \sum_{f_1 f_2 f_3} {}^{\mathrm{A}}C_{[3]}(f_1 f_2 f_3)\,|f_1 f_2 f_3\rangle_{\mathrm{OF}} \\ &= \sum_{f_1 f_2 f_3} {}^{\mathrm{A}}C_{[3]}(f_1 f_2 f_3)\,|f_1 f_2 f_3\rangle_F \times \Phi^{\mathrm{A}}_{3q}(\boldsymbol{r}_1, f_1; \boldsymbol{r}_2, f_2; \boldsymbol{r}_3, f_3)\,. \end{aligned} \tag{15}$$

The wave functions for baryon decuplet with spin $S = \frac{3}{2}$ used in the present calculation in flavor and spin spaces are listed in Tables 3 and 4, respectively.

Table 3. The spin wave function for baryon with spin $S = \frac{3}{2}$.

Spin	$\|S, M_s\rangle$	$[\mathbf{3}]_{\mathbf{S}}$
$\mathrm{S} = \frac{3}{2}$	$\|\frac{3}{2}, \frac{3}{2}\rangle$	$\|\uparrow\uparrow\uparrow\rangle$
	$\|\frac{3}{2}, \frac{1}{2}\rangle$	$\sqrt{\frac{1}{3}}\|\uparrow\uparrow\downarrow + \uparrow\downarrow\uparrow + \downarrow\uparrow\uparrow\rangle$
	$\|\frac{3}{2}, -\frac{1}{2}\rangle$	$\sqrt{\frac{1}{3}}\|\uparrow\downarrow\downarrow + \downarrow\uparrow\downarrow + \downarrow\downarrow\uparrow\rangle$
	$\|\frac{3}{2}, -\frac{3}{2}\rangle$	$\|\downarrow\downarrow\downarrow\rangle$

Table 4. The flavor wave function for the baryon decuplet.

Isospin	$\|T, M_T\rangle$	$[\mathbf{3}]_{\mathbf{F}}$	**Decuplet**
$T = \frac{3}{2}$	$\|\frac{3}{2}, \frac{3}{2}\rangle$	$\|uuu\rangle$	Δ^{++}
	$\|\frac{3}{2}, \frac{1}{2}\rangle$	$\sqrt{\frac{1}{3}}\|uud + udu + duu\rangle$	Δ^{+}
	$\|\frac{3}{2}, -\frac{1}{2}\rangle$	$\sqrt{\frac{1}{3}}\|udd + dud + ddu\rangle$	Δ^{0}
	$\|\frac{3}{2}, -\frac{3}{2}\rangle$	$\|ddd\rangle$	Δ^{-}
$T = 1$	$\|1, 1\rangle$	$\sqrt{\frac{1}{3}}\|uus + usu + suu\rangle$	Σ^{*+}
	$\|1, 0\rangle$	$\sqrt{\frac{1}{6}}\|uds + dus + usd + sud + dsu + sdu\rangle$	Σ^{*0}
	$\|1, -1\rangle$	$\sqrt{\frac{1}{3}}\|dds + dsd + sdd\rangle$	Σ^{*-}
$T = \frac{1}{2}$	$\|\frac{1}{2}, \frac{1}{2}\rangle$	$\sqrt{\frac{1}{3}}\|uss + sus + ssu\rangle$	Ξ^{*0}
	$\|\frac{1}{2}, -\frac{1}{2}\rangle$	$\sqrt{\frac{1}{3}}\|dss + sds + ssd\rangle$	Ξ^{*-}
$T = 0$	$\|0, 0\rangle$	sss	Ω^{-}

2.4. Resonating Group Method

We employ the resonating group method to study the property of the two-cluster system, which is a standard method used in nuclear physics. As usual, the generating coordinate method (GCM), which is equivalent to RGM, was employed in the actual

calculation. The the unknown relative orbital wave function is expanded by using the locally peaked Gaussian basis function [62–65], which is written as

$$\Psi_{6q} = \sum_{i=1}^{N} c_i \mathcal{A} \Phi_{6q}(123, 456, \boldsymbol{s}_i) , \tag{16}$$

with

$$\Phi_{6q}(123, 456, \boldsymbol{s}_i) = \sum_{f_1 f_2 f_3} \prod_{k=1}^{3} \Phi(\boldsymbol{r}_k, \frac{\mu_{AB}}{M_A} \boldsymbol{s}_i) \chi^{\text{sfc}}(123) \sum_{f_4 f_5 f_6} \prod_{n=4}^{6} \Phi(\boldsymbol{r}_n, -\frac{\mu_{AB}}{M_B} \boldsymbol{s}_i) \chi^{\text{sfc}}(456) , \tag{17}$$

where

$$\Phi(\boldsymbol{r}_k, \frac{\mu_{AB}}{M_A} \boldsymbol{s}_i) = \left(\frac{m_k \omega}{\pi}\right)^{3/4} \exp\left[-\frac{1}{2} m_k \omega \left(\boldsymbol{r}_k - \frac{\mu_{AB}}{M_A} \boldsymbol{s}_i\right)^2\right] \tag{18}$$

and ω is the oscillator frequency; $\boldsymbol{s}_i$ $(i = 1, \cdots, N)$ is the generator coordinate, which qualitatively describes the distance between two interacting clusters; M_A and M_B are the masses of cluster A and B, respectively; the reduced mass $\mu_{\text{AB}} = \frac{M_{\text{A}} M_{\text{B}}}{M_{\text{A}} + M_{\text{B}}}$; and χ^{sfc} is the wave function in sfc space.

We define the antisymmetrizing operator of Equation (16) between clusters A and B:

$$\mathcal{A} = 1 - \sum_{i=1}^{3} \sum_{j=4}^{6} P_{ij}^{\text{osfc}} , \tag{19}$$

where P_{ij}^{osfc} is the permutation operator between the ith quark (inside cluster A) and the jth quark (inside cluster B) in orbital, spin, flavor and color space. Due to the permutation symmetry [66], the above equation can be further written as

$$\mathcal{A} = 1 - 9 P_{36}^{\text{osfc}} , \tag{20}$$

and that is why we only need to compute the interaction RGM matrix elements shown in Figure 1, which include the limited direct and exchange terms. Finally, we can dynamically solve the variational equation:

$$\langle \delta \Psi_{6q} | H - E | \Psi_{6q} \rangle = 0 \tag{21}$$

for the bound state problem, and then obtain the binding energy and wave function. Actually, similarly to our previous work [47], a secular equation is deduced from Equation (21) in the calculation:

$$\sum_{j=1}^{10} [H_{ij} - E N_{ij}] c_j = 0 \qquad (i = 1, 2, \cdots, 10)$$

Then, we further project it to partial waves as

$$\sum_{j=1}^{10} [H_{ij}^{L} - E N_{ij}^{L}] c_j = 0 , \qquad (i = 1, 2, \cdots, 10) , \tag{22}$$

where

$$\begin{aligned} \left\{ \begin{array}{c} H_{ij}^{L} \\ N_{ij}^{L} \end{array} \right\} &= \int Y_{LM}^{*}(\hat{\boldsymbol{S}}_i) \left\{ \begin{array}{c} H_{ij} \\ N_{ij} \end{array} \right\} Y_{LM}(\hat{\boldsymbol{S}}_j) d\hat{\boldsymbol{S}}_i d\hat{\boldsymbol{S}}_j, \\ \left\{ \begin{array}{c} H_{ij} \\ N_{ij} \end{array} \right\} &= \int \Phi_{6q}(\boldsymbol{r}_1, \boldsymbol{r}_2, \cdots, \boldsymbol{r}_6, \boldsymbol{S}_i) \left\{ \begin{array}{c} H \\ 1 \end{array} \right\} \mathcal{A}\, \Phi_{6q}(\boldsymbol{r}_1, \boldsymbol{r}_2, \cdots, \boldsymbol{r}_6, \boldsymbol{S}_j) \prod_{k=1}^{6} d\boldsymbol{r}_k. \end{aligned} \tag{23}$$

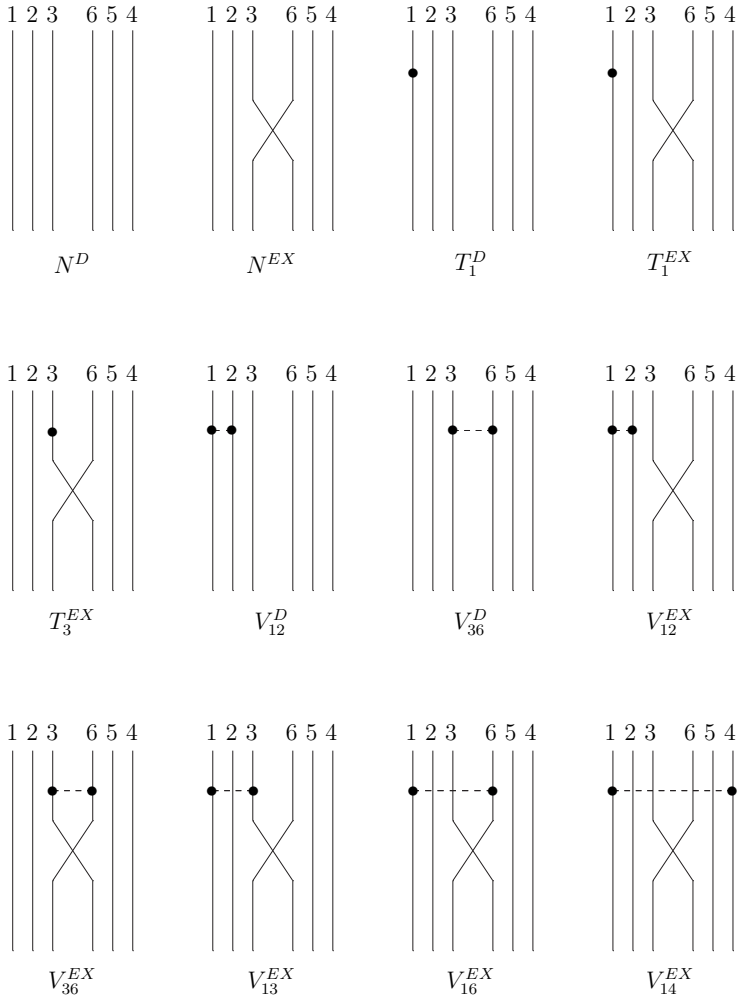

Figure 1. The diagram of RGM matrix elements, including the direct and exchange terms of norm, kinematic and interaction, and the dot denoting the position of quark.

When we further consider the CC channel, Equation (22) is extended into the coupled-channel RGM case:

$$\sum_{j=1}^{20} [H_{ij}^{L} - E N_{ij}^{L}]\, c_j = 0 \qquad (i = 1, \cdots, 20), \tag{24}$$

with $i, j = 1, 2, \cdots, 10$ for the single-channel calculation, and $i, j = 11, 12, \cdots, 20$ for the coupled-channel calculation.

2.5. Model Parameters

In the calculation, only three initial input parameters are actually needed. They are the harmonic oscillator width of an up quark, b_u; the mass of an up quark, m_u; and the mass of a strange quark, m_s.

For the pseudoscalar chiral fields, the masses are taken from [46,47], which correspond the experimental values. For the scalar chiral fields, σ', ε, their masses are taken to be 980 MeV, which correspond to the experimental $a_0(980)$ and $f_0(980)$ mesons. The mass of sigma is decided by fitting the binding energy of deuteron and adopted to be 595 MeV in the present calculation, and the mass of kappa is determined by fitting the nucleon–hyperon scattering processes [46,47]. The cut-off mass Λ is taken to be the value close to the chiral symmetry-breaking-scale [67–69], and we take 1.1 GeV for all chiral fields in order to reduce the number of parameters, as in [46]. It should be mentioned that the effects of SU(2) and SU(3) scalars are not discussed in the present work, or in any of our previous works.

For a strange quark, the harmonic oscillator width is

$$b_i^2 = \frac{1}{m_i \omega} \quad \Rightarrow \quad b_s = b_u \sqrt{\frac{m_u}{m_s}}\,. \tag{25}$$

The coupling constant between the quark and chiral fields is taken to be

$$\frac{g_{ch}^2}{4\pi} = \left(\frac{3}{5}\right)^2 \frac{m_u^2}{M_N^2} \frac{g_{NN\pi}^2}{4\pi} \tag{26}$$

with the empirical value $g_{NN\pi}^2/4\pi = 13.67$ used.

Finally, the one-gluon coupling constants and confinement strengths will be determined by the experimental information in the following way. The experimental energies of the baryon ground states we used are listed in Table 5 for baryons.

Table 5. The experimental energies of the baryon ground states.

	N	Σ	Ξ	Λ	Δ	Σ^*	Ξ^*	Ω
Exp (MeV)	939	1194	1319	1116	1232	1385	1530	1672

The quark gluon coupling constants in Equation (8) are flavor-dependent and can be determined by the following mass split.

$$\begin{aligned} M_\Delta - M_N = 293 \text{ MeV} \quad &\Rightarrow g_u\,, \\ M_\Sigma - M_\Lambda = 78 \text{ MeV} \quad &\Rightarrow g_s\,. \end{aligned} \tag{27}$$

The confinement strengths are fixed by the stability conditions of N, Λ, and Ξ.

$$\begin{aligned} \frac{\partial M_N}{\partial \omega} = 0 \quad &\Rightarrow a_{uu}^c\,, \\ \frac{\partial M_\Lambda}{\partial \omega} = 0 \quad &\Rightarrow a_{us}^c\,, \\ \frac{\partial M_\Xi}{\partial \omega} = 0 \quad &\Rightarrow a_{ss}^c\,. \end{aligned} \tag{28}$$

The zero point energies can be determined by fitting the masses of N, Σ, and $\overline{\Xi + \Omega}$: [47].

$$\begin{aligned} M_N = 939 \text{ MeV} \quad &\Rightarrow a_{uu}^{c0}\,, \\ M_\Sigma = 1194 \text{ MeV} \quad &\Rightarrow a_{us}^{c0}\,, \\ M_\Xi + M_\Omega = 2991 \text{ MeV} \quad &\Rightarrow a_{ss}^{c0}\,. \end{aligned} \tag{29}$$

We list the obtained model parameters in Table 6, and we can see that these parameters are not arbitrarily adjusted.

Table 6. The model parameters and the binding energy of a deuteron. The masses of pseudoscalar chiral fields are $m_\pi = 138$ MeV, $m_K = 495$ MeV, $m_\eta = 549$ MeV, and $m_{\eta'} = 958$ MeV; the masses of scalar chiral fields $m_{\sigma'} = m_\epsilon = m_\kappa = 980$ MeV; the cutoff mass $\Lambda = 1100$ MeV.

b_u	m_u	m_s	m_σ	g_u
0.5 fm	313 MeV	470 MeV	595 MeV	0.886
g_s	$g_{\rm ch}$	a^c_{uu}	a^c_{us}	a^c_{ss}
0.917	2.621	48.1 MeV/ fm^2	60.7 MeV/ fm^2	101.2 MeV/ fm^2
a^{c0}_{uu}	a^{c0}_{us}	a^{c0}_{ss}	$B_{\rm deu}$	
-43.6 MeV	-38.2 MeV	-36.1 MeV	2.15 MeV	

3. In the Single-Channel Calculation

We wanted to dynamically investigate the baryon–baryon interactions in the chiral SU(3) quark model by solving the resonating group method equation, as depicted in Section 2.4. First, we discuss the deuteron structure and compare with the experimental data. Second, the symmetry structure of each dibaryon is analyzed. Then, the dynamical calculations for the single channel are shown for the six chosen dibaryon candidates.

The binding energy and corresponding root-mean-square (RMS) are defined, respectively, just same as in [70]:

$$\begin{aligned} E_b &= -[M_{AB} - (M_A + M_B)]\,, \\ \mathcal{R} &= \sqrt{\frac{1}{6}\sum_{i=1}^{6}\langle(\boldsymbol{r}_i - \boldsymbol{R}_{c.m.})^2\rangle}\,. \end{aligned} \tag{30}$$

3.1. Deuteron

The deuteron, $(NN)_{ST=10}$, is an interesting state. The resultant binding energy, scattering length, and corresponding experimental data [71] are given in Table 7. It is seen that the binding energy is 2.15 MeV and scattering length is 5.49 fm, which are consistent with the experiment.

Table 7. The calculated binding energy and scattering length of the deuteron.

	Theory	**Exp**
binding energy (MeV)	2.15	2.20
scattering length (fm)	5.49	5.42

As discussed in [31], if $\langle \mathcal{A}^{\rm sfc}\rangle \sim 1$, whether this system can be bound depends on the contributions from chiral fields. For the deuteron, the $(NN)_{ST=10}$ state, its $\langle \mathcal{A}^{\rm sfc}\rangle = 10/9$, which just belongs to this case. It is thus very interesting to see which chiral field interactions are important in forming the deuteron. We print out the diagonal GCM matrix elements for the deuteron, of which only the central force from chiral field interactions are shown in Figure 2, where s denotes the generator coordinate with $s_i = s_j = s$ $(i = 1, \cdots, 10)$, the left side of Figure 2 shows the contributions from the pseudoscalar chiral fields, and the right side shows the contributions from the scalar chiral fields. It is seen in Figure 2 that the pseudoscalar pion meson mainly provides the repulsive contribution and the sigma meson mainly provides the attractive contribution, showing clearly that all other chiral field exchanges can be negligible. We should stress that the analysis in Figure 2 is only from central interaction, indicating that the sigma meson exchange mechanism is very

important in helping to form the final deuteron structure, since it provides the attractive interaction. This can be obviously seen from the following calculation for NN scattering process related to the deuteron. In Figure 3, we further show the calculated $^3S_1$ phase shift of the NN interaction, in which the dashed curve denotes the result of closing both sigma meson exchange and tensor coupling; the dashdotted curve shows the result with sigma meson exchange and without tensor coupling; the solid curve represents the result of the full calculation, which means that both the sigma meson exchange and tensor coupling are included. The experimental data were adopted from [72]. From Figure 3, we can see clearly that both contributions from sigma meson exchange and from tensor coupling of $^3S_1$-$^3D_1$ are important in forming the deuteron structure; in particular, the sigma meson exchange largely provides the attractive contribution. Actually, similar results were obtained in [73], in which we also showed the relative wave functions of the deuteron in the chiral SU(3) quark model, including $^3S_1$ and $^3D_1$ in Figure 1.

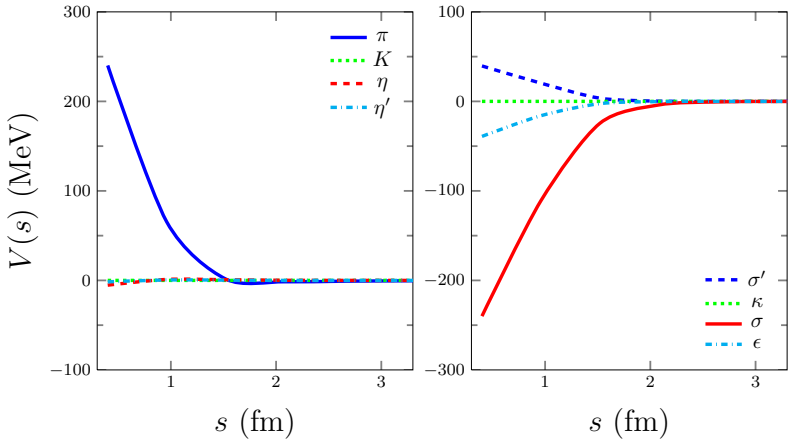

Figure 2. The GCM matrix elements of central force from chiral field interactions.

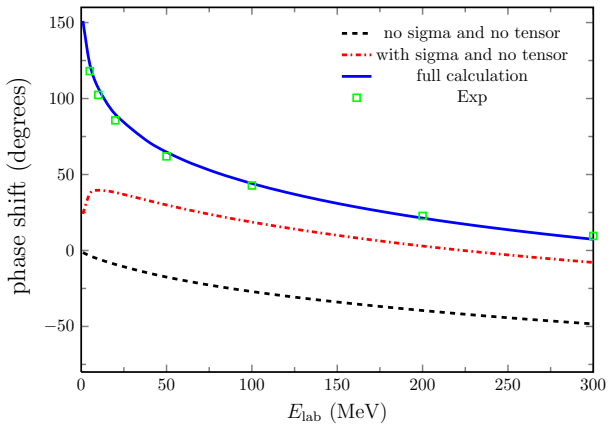

Figure 3. The $^3S_1$ phase shift of the NN scattering.

3.2. Symmetry Property

As discussed in [31], there are two important factors to deciding on whether a baryon-baryon system is bound or not. The first is the symmetry structure, which is characterized by the expectation value of the antisymmetrizer in the sfc space. The second is the interactions of two baryons, which mainly form the quark chiral SU(3) field interactions. The expectation value of $\langle \mathcal{A}^{\rm sfc} \rangle$ for deuteron and the six interesting states are tabulated in Table 8. We also list the corresponding quantum numbers of spin S and isospin T for the two coupled baryons.

If $\langle \mathcal{A}^{\rm sfc} \rangle \sim 0$, it means that this state is almost forbidden and struggles to become a bound state; if $\langle \mathcal{A}^{\rm sfc} \rangle \sim 1$, it means that the contributions from chiral fields are important in forming a bound state; if $\langle \mathcal{A}^{\rm sfc} \rangle \sim 2$, it means that this state is the mostly antisymmetric and symmetric in the sfc space and in orbital space, respectively. Hence, it is very possible to become a bound state in this case. Except the deuteron, it is shown in Table 8 that there are six candidates which belong to this case.

We wanted to understand how the symmetry property affects the binding energy. We drew the diagonal GCM matrix elements for the kinetic energy part in Figure 4. As the kinetic energy itself is spin-flavor-color independent, it is interesting to see the attraction arising from the quark exchange. We performed a systematic analysis for all the interesting systems, including the $\Delta\Delta$, $\Sigma^*\Delta$, $\Xi^*\Omega$ and $\Omega\Omega$ systems, which are spin and isospin-independent. For a clear comparison, we also show the deuteron case in the same figure. The expectation value of the antisymmetrizer is $\langle \mathcal{A}^{\rm sfc} \rangle = 10/9$ for the deuteron, $\langle \mathcal{A}^{\rm sfc} \rangle = 2$ for $\Delta\Delta$, in $\Sigma^*\Delta$, $\Xi^*\Omega$ and $\Omega\Omega$ systems. Taking an example, for the $\Omega\Omega$ with strangeness -6 case, it is shown from Figure 4 that there is strong attraction in the short-range part arising from the quark exchange in the kinetic energy part, and the attraction is small in the relatively long-range part in the deuteron case, which demonstrates clearly that the quantum mechanical effect alone has played a decisive role in binding the two clusters. Similar curves also occur for $\Delta\Delta$, $\Sigma^*\Delta$ and $\Xi^*\Omega$, corresponding to strangeness 0, -1 and -5 cases, respectively.

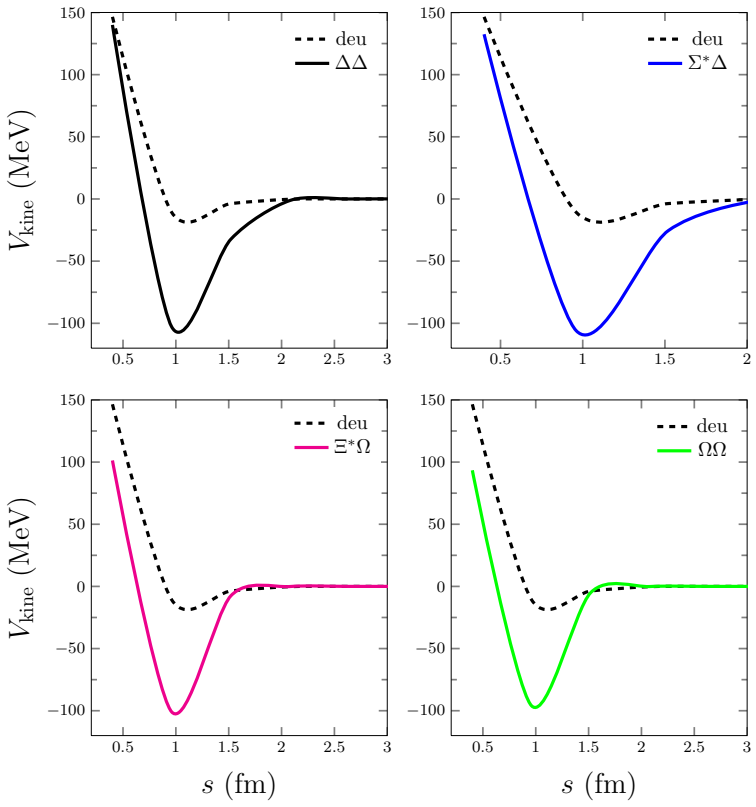

Figure 4. The GCM matrix elements of kinetic energy part for different dibaryon states and deuteron states.

Table 8. The symmetry structure.

	$\langle P_{36}^{\mathrm{sfc}} \rangle$	$\langle \mathcal{A}^{\mathrm{sfc}} \rangle$
deuteron	$-\frac{1}{81}$	$\frac{10}{9}$
$(\Delta\Delta)_{ST=03}$	$-\frac{1}{9}$	2
$(\Delta\Delta)_{ST=30}$	$-\frac{1}{9}$	2
$(\Sigma^*\Delta)_{ST=0\frac{5}{2}}$	$-\frac{1}{9}$	2
$(\Sigma^*\Delta)_{ST=3\frac{1}{2}}$	$-\frac{1}{9}$	2
$(\Xi^*\Omega)_{ST=0\frac{1}{2}}$	$-\frac{1}{9}$	2
$(\Omega\Omega)_{ST=00}$	$-\frac{1}{9}$	2

3.3. Explanation of the deuteron

We provide some explanatory parts of why the deuteron would form in our chiral quark model. As mentioned above, according to the traditional quark model, a baryon is composed of three quarks. The proton and neutron are shown in Figure 5.

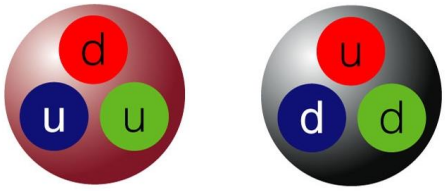

Figure 5. The proton (**left**) and neutron (**right**).

It is shown that the proton has two u quarks and one d quark, and the neutron has two d quarks and one u quark; the corresponding flavor wave functions are given in Table 1. Both protons and neutrons are color singlets; the color wave function is shown in Equation (12). Naturally, one may ask what will happen when a proton and neutron meet together. The experiment has told us that when a proton and a neutron meet together, they become a loosely bound state with a small binding energy, that is, the deuteron, a well established molecular state. We have provided the perfect explanation of why deuteron would be formed within the chiral SU(3) quark model in Section 3.1. It is noted that both contributions—from sigma meson exchange and tensor coupling—are important in forming the deuteron structure. In particular, the sigma meson exchange is largely responsible for the attractive interaction.

3.4. Dibayons

Exploring dibaryon candidates has attracted much attention both theoretically and experimentally. This is a good place to investigate the quark behavior in the short-distance range, since all six quarks would be in a small region where the one gluon exchange and quark exchange play significant roles. The chiral SU(3) quark model is one of the most successful models, in which we can reasonably explain the binding energies of baryon ground states and deuteron; we can also reproduce the NN scattering phase shifts and YN cross-sections [47]. No doubt, predicting possible dibaryon candidates using the same set of parameters in the chiral SU(3) quark model is quite reasonable and meaningful.

We dynamically solved the RGM equation in the chiral SU(3) quark model, and the final results are shown in Table 9, including the binding energy and RMS.

Table 9. The binding energy and RMS in the single-channel case.

	E_b (MeV)	$\mathcal{R}$ (fm)
$(\Delta\Delta)_{ST=30}$	28.9	0.96
$(\Delta\Delta)_{ST=03}$	22.6	1.03
$(\Sigma^*\Delta)_{ST=3\frac{1}{2}}$	34.0	0.90
$(\Sigma^*\Delta)_{ST=0\frac{5}{2}}$	32.3	0.94
$(\Xi^*\Omega)_{ST=0\frac{1}{2}}$	100.9	0.70
$(\Omega\Omega)_{ST=00}$	122.8	0.66

It is seen in Table 9 that all these six candidates would become bound states in the single-channel calculation. We should mention the two reasons of why they all become bound states. One is the symmetry property: they all belong to the $\langle \mathcal{A}^{\rm sfc} \rangle = 2$ case. Another reason is that the scalar meson exchanges mainly dominate the binding behavior. The obtained results are similar to those in [31].

We have noticed that the recent HAL QCD Collaboration reported the $(\Omega\Omega)_{ST=00}$ interaction potential by the lattice QCD simulations. The authors predict that this state would be bound, but with the binding energy of a few MeV [7]. However, we predict that this state would be deeply bound in the chiral SU(3) quark model [29–31], as shown in Table 9, with a binding energy of a hundred MeV. Undoubtedly, this involves the question of interaction mechanism. It is also very interesting to see which chiral field interactions is important in forming the $(\Omega\Omega)_{ST=00}$ dibaryon. We drew the diagonal GCM matrix elements in Figure 6, including the contributions from the pseudoscalar chiral fields and from the scalar chiral fields. It is noticed that the contributions from the scalar sigma and epsilon chiral fields, especially the sigma field, are very important in forming this deeply bound state.

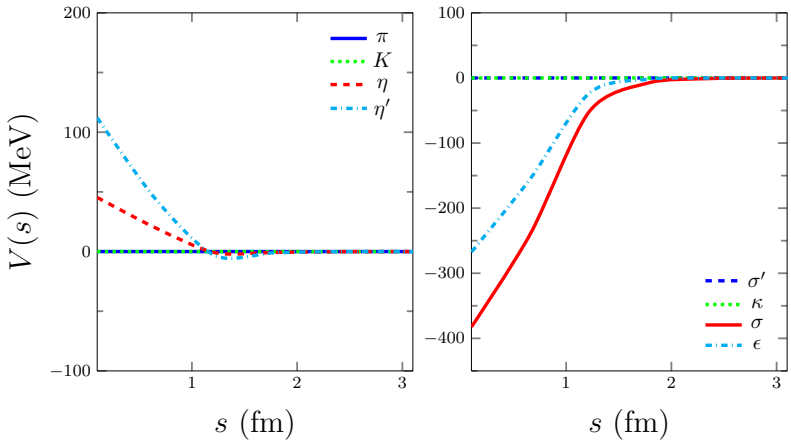

Figure 6. The GCM matrix elements of chiral field interactions for $(\Omega\Omega)_{ST=00}$ dibaryon.

4. In the Coupled-Channel Calculation

We wanted to extend the dynamical calculations in the coupled-channel case. The CC channel was included to investigate other interesting candidates, since we found that CC channel plays an important role in the binding behavior of the d^* system [38,39]. Further exploring the effect from CC channel is surely interesting and important.

It is rather complicated to construct the CC wave function and evaluate the coefficients by using cfp method in group theory. In this section, we develop the method, which is used in studying the $\Delta\Delta$ system, into systems with different strangeness. With this method,

it is relatively easy to construct the CC wave function. By using this method, we further evaluate all the sfc matrix elements needed in the dynamical calculations.

It should be specially emphasized that in the present calculations, we only consider the following configuration for each state: ($\Delta\Delta$+CC), ($\Sigma^*\Delta$+CC), ($\Xi^*\Omega$+CC), or ($\Omega\Omega$+CC), respectively.

4.1. $(\Delta\Delta)_{ST=30}$

The CC wave function can be written as

$$|\mathrm{CC}\rangle_{ST=30} = -\frac{1}{2}\,|\Delta\Delta\rangle_{ST=30} + \frac{5}{2}\,\mathcal{A}^{\mathrm{sfc}}|\Delta\Delta\rangle_{ST=30} \tag{31}$$

Then according to Equation (31) all the sfc matrix elements for the $(\Delta\Delta)_{ST=30}$ state are computed and listed in Table 10, including $\langle\Delta\Delta|\hat{O}_{ij}|\Delta\Delta\rangle$, $\langle\Delta\Delta|\hat{O}_{ij}|\mathrm{CC}\rangle$ and $\langle\mathrm{CC}|\hat{O}_{ij}|\mathrm{CC}\rangle$. These results are similar to those in [38]. We can see that the $\langle\mathrm{CC}|\lambda_1^c\cdot\lambda_2^c|\mathrm{CC}\rangle = -\frac{2}{3}$, indicating that the CC state is correct and consistent with those in group theory [50].

Table 10. The matrix elements of the $(\Delta\Delta)_{ST=30}$ state in sfc space.

		$\Delta\Delta$ $\Delta\Delta$	$\Delta\Delta$ CC	CC CC		$\Delta\Delta$ $\Delta\Delta$	$\Delta\Delta$ CC	CC CC
1		1	0	1				
P_{36}		$-\frac{1}{9}$	$-\frac{4}{9}$	$-\frac{7}{9}$				
$\lambda_i^c\cdot\lambda_j^c$	$\hat{O}_{12}$	$-\frac{8}{3}$	0	$-\frac{2}{3}$	$\hat{O}_{36}$	0	0	$-\frac{4}{3}$
	$\hat{O}_{12}P_{36}$	$\frac{8}{27}$	$\frac{32}{27}$	$\frac{2}{27}$	$\hat{O}_{36}P_{36}$	$-\frac{16}{27}$	$\frac{8}{27}$	$\frac{32}{27}$
	$\hat{O}_{13}P_{36}$	$\frac{8}{27}$	$\frac{32}{27}$	$\frac{20}{27}$	$\hat{O}_{16}P_{36}$	$\frac{8}{27}$	$-\frac{4}{27}$	$\frac{20}{27}$
	$\hat{O}_{14}P_{36}$	$-\frac{4}{27}$	$\frac{2}{27}$	$\frac{35}{27}$				
$\sigma_i\cdot\sigma_j\,\lambda_i^c\cdot\lambda_j^c$	$\hat{O}_{12}$	$-\frac{8}{3}$	0	$-\frac{2}{3}$	$\hat{O}_{36}$	0	0	$-\frac{4}{3}$
	$\hat{O}_{12}P_{36}$	$\frac{8}{27}$	$\frac{32}{27}$	$\frac{2}{27}$	$\hat{O}_{36}P_{36}$	$-\frac{16}{27}$	$\frac{8}{27}$	$\frac{32}{27}$
	$\hat{O}_{13}P_{36}$	$\frac{8}{27}$	$\frac{32}{27}$	$\frac{20}{27}$	$\hat{O}_{16}P_{36}$	$\frac{8}{27}$	$-\frac{4}{27}$	$\frac{20}{27}$
	$\hat{O}_{14}P_{36}$	$-\frac{4}{27}$	$\frac{2}{27}$	$\frac{35}{27}$				
$\sigma_i\cdot\sigma_j\,\sum_{a=1}^{3}\lambda_a(i)\lambda_a(j)$	$\hat{O}_{12}$	1	0	-1	$\hat{O}_{36}$	$-\frac{5}{3}$	0	$-\frac{1}{3}$
	$\hat{O}_{12}P_{36}$	$-\frac{1}{9}$	$-\frac{4}{9}$	$\frac{11}{9}$	$\hat{O}_{36}P_{36}$	$\frac{7}{9}$	$\frac{4}{9}$	$\frac{1}{9}$
	$\hat{O}_{13}P_{36}$	$-\frac{1}{9}$	$-\frac{4}{9}$	$\frac{5}{9}$	$\hat{O}_{16}P_{36}$	$-\frac{1}{9}$	$\frac{8}{9}$	$\frac{5}{9}$
	$\hat{O}_{14}P_{36}$	$\frac{1}{3}$	$\frac{2}{3}$	0				
$\sigma_i\cdot\sigma_j\,\sum_{a=4}^{7}\lambda_a(i)\lambda_a(j)$	$\hat{O}_{12}$	0	0	0	$\hat{O}_{36}$	0	0	0
	$\hat{O}_{12}P_{36}$	0	0	0	$\hat{O}_{36}P_{36}$	0	0	0
	$\hat{O}_{13}P_{36}$	0	0	0	$\hat{O}_{16}P_{36}$	0	0	0
	$\hat{O}_{14}P_{36}$	0	0	0				

After including the CC channel, we dynamically solve the corresponding coupled-channel equation in the chiral SU(3) quark model; the results of the coupled-channel calculation are shown in Table 11. We notice that the couplings from tensor interaction and from CC channel add increments of about 6.2 MeV and 17.4 MeV to the binding energy,

respectively. Both couplings make the binding energy increase from 22.7 MeV to 47.4 MeV, and the RMS decreases from 0.98 fm to 0.88 fm.

Table 11. The binding energy and RMS in the coupled-channel case for the $(\Delta\Delta)_{ST=30}$ state.

	$L=0$		$L=0+2$	
	ΔΔ	**ΔΔ + CC**	**ΔΔ**	**ΔΔ + CC**
E_b (MeV)	22.7	40.1	28.9	47.7
$\mathcal{R}$ (fm)	0.98	0.89	0.96	0.88

We present the results calculated in the extended chiral SU(3) quark model [39] in Table 12. We can see that the binding energy increases from 56.1 MeV to 84 MeV, and RMS decreases from 0.84 fm to 0.78 fm, indicating that this state is deeply bound and the coupling to the CC channel plays a significant role. It can also be seen that the mass of this state is higher than the mass of $N\Delta\pi$ and lower than the threshold of the $\Delta\Delta$ channel.

Table 12. The same as Table 11 but in the extended chiral SU(3)quark model.

	$L=0$		$L=0+2$	
	ΔΔ	**ΔΔ + CC**	**ΔΔ**	**ΔΔ + CC**
E_b (MeV)	56.1	62.4	78.2	84.0
$\mathcal{R}$ (fm)	0.84	0.84	0.78	0.78

The width was further evaluated by using the above obtained CC wave function in the extended chiral SU(3) quark model. The results show that the resultant total width for this state is about 69 MeV [44], which is compatible with the experimental observation of about 75 MeV [1].

4.2. $(\Delta\Delta)_{ST=03}$

The obtained CC wave function is

$$|\mathrm{CC}\rangle_{ST=03} = -\frac{1}{2}\,|\Delta\Delta\rangle_{ST=03} + \frac{5}{2}\,\mathcal{A}^{\mathrm{sfc}}|\Delta\Delta\rangle_{ST=03} \tag{32}$$

Then according to Equation (32) all the sfc matrix elements for the $(\Delta\Delta)_{ST=03}$ state are computed and listed in Table 13. These results are similar to those in [10]. It is noted that the $\langle \mathrm{CC}|\lambda_1^c \cdot \lambda_2^c|\mathrm{CC}\rangle = -\frac{2}{3}$, verifying again that the CC is correct.

Similarly, we performed the corresponding coupled-channel calculation dynamically in the chiral SU(3) quark model. The calculated results are given in Table 14. There is no tensor force in this case, due to its $S = 0$ state. It is noticed that the coupling from CC channel increases the binding energy from 22.6 MeV to 31.6 MeV, and the RMS decreases from 1.03 fm to 0.97 fm, which indicates that the CC channel coupling has a large effect on the $(\Delta\Delta)_{ST=03}$ state. The mass of this state is higher than the mass of $N\Delta\pi$ and lower than the threshold of the $\Delta\Delta$ channel.

Table 13. The same as Table 10 but for the $(\Delta\Delta)_{ST=03}$ state.

		$\Delta\Delta$ $\Delta\Delta$	$\Delta\Delta$ CC	CC CC		$\Delta\Delta$ $\Delta\Delta$	$\Delta\Delta$ CC	CC CC
1		1	0	1				
P_{36}		$-\frac{1}{9}$	$-\frac{4}{9}$	$-\frac{7}{9}$				
$\lambda_i^c \cdot \lambda_j^c$	$\hat{O}_{12}$	$-\frac{8}{3}$	0	$-\frac{2}{3}$	$\hat{O}_{36}$	0	0	$-\frac{4}{3}$
	$\hat{O}_{12}P_{36}$	$\frac{8}{27}$	$\frac{32}{27}$	$\frac{2}{27}$	$\hat{O}_{36}P_{36}$	$-\frac{16}{27}$	$\frac{8}{27}$	$\frac{32}{27}$
	$\hat{O}_{13}P_{36}$	$\frac{8}{27}$	$\frac{32}{27}$	$\frac{20}{27}$	$\hat{O}_{16}P_{36}$	$\frac{8}{27}$	$-\frac{4}{27}$	$\frac{20}{27}$
	$\hat{O}_{14}P_{36}$	$-\frac{4}{27}$	$\frac{2}{27}$	$\frac{35}{27}$				
$\sigma_i \cdot \sigma_j \, \lambda_i^c \cdot \lambda_j^c$	$\hat{O}_{12}$	$-\frac{8}{3}$	0	$-\frac{10}{3}$	$\hat{O}_{36}$	0	$-\frac{16}{9}$	$-\frac{20}{9}$
	$\hat{O}_{12}P_{36}$	$\frac{8}{27}$	$\frac{32}{27}$	$\frac{74}{27}$	$\hat{O}_{36}P_{36}$	$\frac{112}{27}$	$-\frac{8}{27}$	$\frac{88}{27}$
	$\hat{O}_{13}P_{36}$	$\frac{8}{27}$	$\frac{32}{27}$	$\frac{68}{27}$	$\hat{O}_{16}P_{36}$	$\frac{8}{27}$	$\frac{44}{27}$	$\frac{68}{27}$
	$\hat{O}_{14}P_{36}$	$\frac{4}{9}$	$\frac{14}{9}$	$\frac{7}{3}$				
$\sigma_i \cdot \sigma_j \sum_{a=1}^{3} \lambda_a(i)\lambda_a(j)$	$\hat{O}_{12}$	1	0	-1	$\hat{O}_{36}$	$-\frac{5}{3}$	0	$-\frac{1}{3}$
	$\hat{O}_{12}P_{36}$	$-\frac{1}{9}$	$-\frac{4}{9}$	$\frac{11}{9}$	$\hat{O}_{36}P_{36}$	$\frac{7}{9}$	$\frac{4}{9}$	$\frac{1}{9}$
	$\hat{O}_{13}P_{36}$	$-\frac{1}{9}$	$-\frac{4}{9}$	$\frac{5}{9}$	$\hat{O}_{16}P_{36}$	$-\frac{1}{9}$	$\frac{8}{9}$	$\frac{5}{9}$
	$\hat{O}_{14}P_{36}$	$\frac{1}{3}$	$\frac{2}{3}$	0				
$\sigma_i \cdot \sigma_j \sum_{a=4}^{7} \lambda_a(i)\lambda_a(j)$	$\hat{O}_{12}$	0	0	0	$\hat{O}_{36}$	0	0	0
	$\hat{O}_{12}P_{36}$	0	0	0	$\hat{O}_{36}P_{36}$	0	0	0
	$\hat{O}_{13}P_{36}$	0	0	0	$\hat{O}_{16}P_{36}$	0	0	0
	$\hat{O}_{14}P_{36}$	0	0	0				

Table 14. The same as Table 11 but for the $(\Delta\Delta)_{ST=03}$ state.

	$L = 0$	
	ΔΔ	**ΔΔ + CC**
E_b (MeV)	22.6	31.6
$\mathcal{R}$ (fm)	1.03	0.97

4.3. $(\Sigma^*\Delta)_{ST=3\frac{1}{2}}$

Now we move to the system with strangeness -1, choosing $\Sigma^*\Delta$ with spin $S = 3$ case. The Σ^* baryon has a strange quark. As in [38], a method was developed to build the CC wave function for $\Sigma^*\Delta$ system, which is written as

$$|\mathrm{CC}\rangle_{ST=3\frac{1}{2}} = a\,|\Sigma^*\Delta\rangle_{ST=3\frac{1}{2}} + b\,\mathcal{A}^{\mathrm{sfc}}|\Sigma^*\Delta\rangle_{ST=3\frac{1}{2}}\,, \tag{33}$$

and by utilizing the orthogonality $\langle\Sigma^*\Delta|CC\rangle = 0$, $\langle CC|CC\rangle = 1$, we obtain $a = -\frac{1}{2}$, $b = \frac{5}{2}$; thus,

$$|\mathrm{CC}\rangle_{ST=3\frac{1}{2}} = -\frac{1}{2}\,|\Sigma^*\Delta\rangle_{ST=3\frac{1}{2}} + \frac{5}{2}\,\mathcal{A}^{\mathrm{sfc}}|\Sigma^*\Delta\rangle_{ST=3\frac{1}{2}}\,. \tag{34}$$

Then according to Equation (34) all the sfc matrix elements are evaluated and tabulated in Table 15, including $\langle\Sigma^*\Delta|\hat{O}_{ij}|\Sigma^*\Delta\rangle$, $\langle\Sigma^*\Delta|\hat{O}_{ij}|\mathrm{CC}\rangle$ and $\langle\mathrm{CC}|\hat{O}_{ij}|\mathrm{CC}\rangle$. It is noticed again that in this extended system with strangeness -1, the $\langle CC|\lambda_1^c\cdot\lambda_2^c|CC\rangle = -\frac{2}{3}$, indicating the correctness of constructed CC wave function.

Table 15. The same as Table 10 but for the $(\Sigma^*\Delta)_{ST=3\frac{1}{2}}$ state.

		$\Sigma^*\Delta$ $\Sigma^*\Delta$	$\Sigma^*\Delta$ CC	CC CC		$\Sigma^*\Delta$ $\Sigma^*\Delta$	$\Sigma^*\Delta$ CC	CC CC
1		1	0	1				
P_{36}		$-\frac{1}{9}$	$-\frac{4}{9}$	$-\frac{7}{9}$				
$\lambda_i^c\cdot\lambda_j^c$	$\hat{O}_{12}$	$-\frac{8}{3}$	0	$-\frac{2}{3}$	$\hat{O}_{36}$	0	0	$-\frac{4}{3}$
	$\hat{O}_{12}P_{36}$	$\frac{8}{27}$	$\frac{32}{27}$	$\frac{2}{27}$	$\hat{O}_{36}P_{36}$	$-\frac{16}{27}$	$\frac{8}{27}$	$\frac{32}{27}$
	$\hat{O}_{13}P_{36}$	$\frac{8}{27}$	$\frac{32}{27}$	$\frac{20}{27}$	$\hat{O}_{16}P_{36}$	$\frac{8}{27}$	$-\frac{4}{27}$	$\frac{20}{27}$
	$\hat{O}_{14}P_{36}$	$-\frac{4}{27}$	$\frac{2}{27}$	$\frac{35}{27}$				
$\sigma_i\cdot\sigma_j\,\lambda_i^c\cdot\lambda_j^c$	$\hat{O}_{12}$	$-\frac{8}{3}$	0	$-\frac{2}{3}$	$\hat{O}_{36}$	0	0	$-\frac{4}{3}$
	$\hat{O}_{12}P_{36}$	$\frac{8}{27}$	$\frac{32}{27}$	$\frac{2}{27}$	$\hat{O}_{36}P_{36}$	$-\frac{16}{27}$	$\frac{8}{27}$	$\frac{32}{27}$
	$\hat{O}_{13}P_{36}$	$\frac{8}{27}$	$\frac{32}{27}$	$\frac{20}{27}$	$\hat{O}_{16}P_{36}$	$\frac{8}{27}$	$-\frac{4}{27}$	$\frac{20}{27}$
	$\hat{O}_{14}P_{36}$	$-\frac{4}{27}$	$\frac{2}{27}$	$\frac{35}{27}$				
$\sigma_i\cdot\sigma_j\,\sum_{a=1}^{3}\lambda_a(i)\lambda_a(j)$	$\hat{O}_{12}$	$\frac{2}{3}$	0	$-\frac{2}{3}$	$\hat{O}_{36}$	$-\frac{10}{9}$	0	$-\frac{2}{9}$
	$\hat{O}_{12}P_{36}$	$-\frac{2}{27}$	$-\frac{8}{27}$	$\frac{22}{27}$	$\hat{O}_{36}P_{36}$	$\frac{14}{27}$	$\frac{8}{27}$	$\frac{2}{27}$
	$\hat{O}_{13}P_{36}$	$-\frac{2}{27}$	$-\frac{8}{27}$	$\frac{10}{27}$	$\hat{O}_{16}P_{36}$	$-\frac{2}{27}$	$\frac{16}{27}$	$\frac{10}{27}$
	$\hat{O}_{14}P_{36}$	$\frac{2}{9}$	$\frac{4}{9}$	0				
$\sigma_i\cdot\sigma_j\,\sum_{a=4}^{7}\lambda_a(i)\lambda_a(j)$	$\hat{O}_{12}$	$\frac{2}{3}$	0	0	$\hat{O}_{36}$	$-\frac{2}{9}$	0	$\frac{2}{9}$
	$\hat{O}_{12}P_{36}$	$-\frac{2}{27}$	$-\frac{8}{27}$	$\frac{4}{27}$	$\hat{O}_{36}P_{36}$	$\frac{2}{9}$	0	$-\frac{2}{9}$
	$\hat{O}_{13}P_{36}$	$-\frac{2}{27}$	$-\frac{8}{27}$	$-\frac{2}{27}$	$\hat{O}_{16}P_{36}$	$-\frac{2}{27}$	$\frac{4}{27}$	$-\frac{2}{27}$
	$\hat{O}_{14}P_{36}$	$\frac{2}{27}$	$\frac{2}{27}$	$-\frac{2}{27}$				

By applying these sfc matrix elements, we dynamically solved the corresponding coupled-channel equation. The calculated results are given in Table 16. We see again that the coupling from tensor interaction and from the CC channel resulted in increments of about 3.6 MeV and 14.8 MeV to the binding energy, respectively. Both couplings make the binding energy increase from 30.4 MeV to 50.4 MeV and RMS decrease from 0.91 fm to 0.84 fm, showing this state is deeply bound, and the coupling to the CC channel plays a significant role. We can see that the mass of this state is higher than the mass of $\Lambda\pi\Delta$ and lower than the threshold of the $\Sigma^*\Delta$ channel.

Table 16. The same as Table 11 but for the $(\Sigma^*\Delta)_{ST=3\frac{1}{2}}$ state.

	$L=0$		$L=0+2$	
	$\Sigma^*\Delta$	$\Sigma^*\Delta$+CC	$\Sigma^*\Delta$	$\Sigma^*\Delta$ + CC
E_b (MeV)	30.4	45.2	34.0	50.4
$\mathcal{R}$ (fm)	0.91	0.85	0.90	0.84

4.4. $(\Sigma^*\Delta)_{ST=0\frac{5}{2}}$

There is another $\Sigma^*\Delta$ state, but for it, $S=0$; thus, there is no contribution from tensor force to this state. A similar method to that above was utilized to build the CC wave function, and finally, we obtained

$$|\mathrm{CC}\rangle_{ST=0\frac{5}{2}} = -\frac{1}{2}\,|\Sigma^*\Delta\rangle_{ST=0\frac{5}{2}} + \frac{5}{2}\,\mathcal{A}^{\mathrm{sfc}}|\Sigma^*\Delta\rangle_{ST=0\frac{5}{2}}\,, \tag{35}$$

and according to Equation (35) all the sfc matrix elements were computed and listed in Table 17. It can be noted again that $\langle CC|\lambda_1^c\cdot\lambda_2^c|CC\rangle = -\frac{2}{3}$, indicating the correctness of CC wave function in this case.

Table 17. The same as Table 10 but for the $(\Sigma^*\Delta)_{ST=0\frac{5}{2}}$ state.

		$\Sigma^*\Delta$ $\Sigma^*\Delta$	$\Sigma^*\Delta$ CC	CC CC		$\Sigma^*\Delta$ $\Sigma^*\Delta$	$\Sigma^*\Delta$ CC	CC CC
1		1	0	1				
P_{36}		$-\frac{1}{9}$	$-\frac{4}{9}$	$-\frac{7}{9}$				
$\lambda_i^c\cdot\lambda_j^c$	$\hat{O}_{12}$	$-\frac{8}{3}$	0	$-\frac{2}{3}$	$\hat{O}_{36}$	0	0	$-\frac{4}{3}$
	$\hat{O}_{12}P_{36}$	$\frac{8}{27}$	$\frac{32}{27}$	$\frac{2}{27}$	$\hat{O}_{36}P_{36}$	$-\frac{16}{27}$	$\frac{8}{27}$	$\frac{32}{27}$
	$\hat{O}_{13}P_{36}$	$\frac{8}{27}$	$\frac{32}{27}$	$\frac{20}{27}$	$\hat{O}_{16}P_{36}$	$\frac{8}{27}$	$-\frac{4}{27}$	$\frac{20}{27}$
	$\hat{O}_{14}P_{36}$	$-\frac{4}{27}$	$\frac{2}{27}$	$\frac{35}{27}$				
$\sigma_i\cdot\sigma_j\,\lambda_i^c\lambda_j^c$	$\hat{O}_{12}$	$-\frac{8}{3}$	0	$-\frac{10}{3}$	$\hat{O}_{36}$	0	-$\frac{16}{9}$	$-\frac{20}{9}$
	$\hat{O}_{12}P_{36}$	$\frac{8}{27}$	$\frac{32}{27}$	$\frac{74}{27}$	$\hat{O}_{36}P_{36}$	$\frac{112}{27}$	-$\frac{8}{27}$	$\frac{88}{27}$
	$\hat{O}_{13}P_{36}$	$\frac{8}{27}$	$\frac{32}{27}$	$\frac{68}{27}$	$\hat{O}_{16}P_{36}$	$\frac{8}{27}$	$\frac{44}{27}$	$\frac{68}{27}$
	$\hat{O}_{14}P_{36}$	$\frac{4}{9}$	$\frac{14}{9}$	$\frac{7}{3}$				
$\sigma_i\cdot\sigma_j\,\sum_{a=1}^{3}\lambda_a(i)\lambda_a(j)$	$\hat{O}_{12}$	$\frac{2}{3}$	0	$-\frac{2}{3}$	$\hat{O}_{36}$	$-\frac{10}{9}$	0	$-\frac{2}{9}$
	$\hat{O}_{12}P_{36}$	$-\frac{2}{27}$	$-\frac{8}{27}$	$\frac{22}{27}$	$\hat{O}_{36}P_{36}$	$\frac{14}{27}$	$\frac{8}{27}$	$\frac{2}{27}$
	$\hat{O}_{13}P_{36}$	$-\frac{2}{27}$	$-\frac{8}{27}$	$\frac{10}{27}$	$\hat{O}_{16}P_{36}$	$-\frac{2}{27}$	$\frac{16}{27}$	$\frac{10}{27}$
	$\hat{O}_{14}P_{36}$	$\frac{2}{9}$	$\frac{4}{9}$	0				
$\sigma_i\cdot\sigma_j\,\sum_{a=4}^{7}\lambda_a(i)\lambda_a(j)$	$\hat{O}_{12}$	$\frac{2}{3}$	0	$-\frac{2}{3}$	$\hat{O}_{36}$	$-\frac{10}{9}$	0	$-\frac{2}{9}$
	$\hat{O}_{12}P_{36}$	$-\frac{2}{27}$	$-\frac{8}{27}$	$\frac{22}{27}$	$\hat{O}_{36}P_{36}$	$\frac{14}{27}$	$\frac{8}{27}$	$\frac{2}{27}$
	$\hat{O}_{13}P_{36}$	$-\frac{2}{27}$	$-\frac{8}{27}$	$\frac{10}{27}$	$\hat{O}_{16}P_{36}$	$-\frac{2}{27}$	$\frac{16}{27}$	$\frac{10}{27}$
	$\hat{O}_{14}P_{36}$	$\frac{2}{9}$	$\frac{4}{9}$	0				

The corresponding coupled-channel equation was dynamically solved in the chiral SU(3) quark model. The calculated results are given in Table 18. We can see that, due to the coupling from CC channel, the binding energy increases from 32.3 MeV 41.5 MeV, and the RMS decreases from 0.94 fm to 0.90 fm. This indicates that this state is bound, and the coupling to the CC channel has an obvious influence on this state. Again, We can also see that the mass of this state is higher than the mass of $\Lambda\pi\Delta$ and lower than the threshold of $\Sigma^*\Delta$ channel.

Table 18. The same as Table 11 but for the $(\Sigma^*\Delta)_{ST=0\frac{5}{2}}$ state.

	$L=0$	
	$\Sigma^*\Delta$	$\Sigma^*\Delta$ + CC
E_b (MeV)	32.3	41.5
$\mathcal{R}$ (fm)	0.94	0.90

4.5. $(\Xi^*\Omega)_{ST=0\frac{1}{2}}$

Now, we continue to move to a high strangeness(-5) system, $\Xi^*\Omega$ with $S=0$ and $T=1/2$, in which there are two strange quarks in the Ξ^* baryon and three strange quarks in the Ω baryon. We adopted a similar method as in [38] and employed the orthogonality $\langle\Xi^*\Omega|CC\rangle=0$, $\langle CC|CC\rangle=1$; finally, the CC wave function was obtained:

$$|\mathrm{CC}\rangle_{ST=0\frac{1}{2}}=-\frac{1}{2}|\Xi^*\Omega\rangle_{ST=0\frac{1}{2}}+\frac{5}{2}\mathcal{A}^{\mathrm{sfc}}|\Xi^*\Omega\rangle_{ST=0\frac{1}{2}}\,. \tag{36}$$

Then according to Equation (36) all the sfc matrix elements are evaluated and listed in Table 19, including $\langle\Xi^*\Omega|\hat{O}_{ij}|\Xi^*\Omega\rangle$, $\langle\Xi^*\Omega|\hat{O}_{ij}|CC\rangle$ and $\langle CC|\hat{O}_{ij}|CC\rangle$. It is seen that in this case with high strangeness, $\langle CC|\lambda_1^c\cdot\lambda_2^c|CC\rangle=-\frac{2}{3}$, indicating the correctness of constructed CC wave function.

Table 19. The same as Table 10 but for the $(\Xi^*\Omega)_{ST=0\frac{1}{2}}$ state.

		$\Xi^*\Omega$ $\Xi^*\Omega$	$\Xi^*\Omega$ CC	CC CC		$\Xi^*\Omega$ $\Xi^*\Omega$	$\Xi^*\Omega$ CC	CC CC
1		1	0	1				
P_{36}		$-\frac{1}{9}$	$-\frac{4}{9}$	$-\frac{7}{9}$				
$\lambda_i^c\cdot\lambda_j^c$	$\hat{O}_{12}$	$-\frac{8}{3}$	0	$-\frac{2}{3}$	$\hat{O}_{36}$	0	0	$-\frac{4}{3}$
	$\hat{O}_{12}P_{36}$	$\frac{8}{27}$	$\frac{32}{27}$	$\frac{2}{27}$	$\hat{O}_{36}P_{36}$	$-\frac{16}{27}$	$\frac{8}{27}$	$\frac{32}{27}$
	$\hat{O}_{13}P_{36}$	$\frac{8}{27}$	$\frac{32}{27}$	$\frac{20}{27}$	$\hat{O}_{16}P_{36}$	$\frac{8}{27}$	$-\frac{4}{27}$	$\frac{20}{27}$
	$\hat{O}_{14}P_{36}$	$-\frac{4}{27}$	$\frac{2}{27}$	$\frac{35}{27}$				
$\sigma_i\cdot\sigma_j\,\lambda_i^c\cdot\lambda_j^c$	$\hat{O}_{12}$	$-\frac{8}{3}$	0	$-\frac{10}{3}$	$\hat{O}_{36}$	0	$-\frac{16}{9}$	$-\frac{20}{9}$
	$\hat{O}_{12}P_{36}$	$\frac{8}{27}$	$\frac{32}{27}$	$\frac{74}{27}$	$\hat{O}_{36}P_{36}$	$\frac{112}{27}$	$-\frac{8}{27}$	$\frac{88}{27}$
	$\hat{O}_{13}P_{36}$	$\frac{8}{27}$	$\frac{32}{27}$	$\frac{68}{27}$	$\hat{O}_{16}P_{36}$	$\frac{8}{27}$	$\frac{44}{27}$	$\frac{68}{27}$
	$\hat{O}_{14}P_{36}$	$\frac{4}{9}$	$\frac{4}{9}$	$\frac{7}{3}$				

Table 19. *Cont.*

$\sigma_i \cdot \sigma_j \sum_{a=1}^{3} \lambda_a(i)\lambda_a(j)$	$\hat{O}_{12}$	0	0	0	$\hat{O}_{36}$	0	0	0
	$\hat{O}_{12}P_{36}$	0	0	0	$\hat{O}_{36}P_{36}$	0	0	0
	$\hat{O}_{13}P_{36}$	0	0	0	$\hat{O}_{16}P_{36}$	0	0	0
	$\hat{O}_{14}P_{36}$	0	0	0				
$\sigma_i \cdot \sigma_j \sum_{a=4}^{7} \lambda_a(i)\lambda_a(j)$	$\hat{O}_{12}$	$\frac{2}{3}$	0	$-\frac{2}{3}$	$\hat{O}_{36}$	$-\frac{10}{9}$	0	$-\frac{2}{9}$
	$\hat{O}_{12}P_{36}$	$-\frac{2}{27}$	$-\frac{8}{27}$	$\frac{22}{27}$	$\hat{O}_{36}P_{36}$	$\frac{14}{27}$	$\frac{8}{27}$	$\frac{2}{27}$
	$\hat{O}_{13}P_{36}$	$-\frac{2}{27}$	$-\frac{8}{27}$	$\frac{10}{27}$	$\hat{O}_{16}P_{36}$	$-\frac{2}{27}$	$\frac{16}{27}$	$\frac{10}{27}$
	$\hat{O}_{14}P_{36}$	$\frac{2}{9}$	$\frac{4}{9}$	0				

For dynamically solving the corresponding coupled-channel equation, the results are given in Table 20. We notice that no matter whether single-channel or coupled-channel calculations are used, this state will be deeply bound. It is shown that the coupling to the CC channel has some influence in forming this bound state, which results in an increment of about 4.8 MeV to the binding energy, and the RMS decreases from 0.70 fm to 0.69 fm.

Table 20. The same as Table 11 but for the $(\Xi^*\Omega)_{ST=0\frac{1}{2}}$ state.

	$L = 0$	
	$\Xi^*\Omega$	$\Xi^*\Omega$ + CC
E_b (MeV)	100.9	105.7
$\mathcal{R}$ (fm)	0.70	0.69

4.6. $(\Omega\Omega)_{ST=00}$

We continue to extend system with high strangeness, -6; $\Omega\Omega$ with $S = 0, T = 0$. Similarly, we adopted the method utilized in [38] to build the CC wave function. Again the similar orthogonality $\langle \Omega\Omega|CC\rangle = 0, \langle CC|CC\rangle = 1$ was employed. Finally, the CC wave function becomes

$$|\mathrm{CC}\rangle_{ST=00} = -\frac{1}{2}|\Omega\Omega\rangle_{ST=00} + \frac{5}{2}\mathcal{A}^{\mathrm{sfc}}|\Omega\Omega\rangle_{ST=00}\,. \tag{37}$$

Then according to Equation (37) all the sfc matrix elements, including $\langle \Omega\Omega|\hat{O}_{ij}|\Omega\Omega\rangle$, $\langle \Omega\Omega|\hat{O}_{ij}|CC\rangle$, and $\langle CC|\hat{O}_{ij}|CC\rangle$, are further evaluated and tabulated in Table 21. It is noticed that the $\langle CC|\lambda_1^c \cdot \lambda_2^c|CC\rangle = -\frac{2}{3}$, again indicating that in this case with high strangeness, the constructed CC wave function is correct.

Table 21. The same as Table 10 but for the $(\Omega\Omega)_{ST=00}$ state.

		$\Omega\Omega$ $\Omega\Omega$	$\Omega\Omega$ CC	CC CC		$\Omega\Omega$ $\Omega\Omega$	$\Omega\Omega$ CC	CC CC
1		1	0	1				
P_{36}		$-\frac{1}{9}$	$-\frac{4}{9}$	$-\frac{7}{9}$				
$\lambda_i^c \cdot \lambda_j^c$	$\hat{O}_{12}$	$-\frac{8}{3}$	0	$-\frac{2}{3}$	$\hat{O}_{36}$	0	0	$-\frac{4}{3}$
	$\hat{O}_{12}P_{36}$	$\frac{8}{27}$	$\frac{32}{27}$	$\frac{2}{27}$	$\hat{O}_{36}P_{36}$	$-\frac{16}{27}$	$\frac{8}{27}$	$\frac{32}{27}$
	$\hat{O}_{13}P_{36}$	$\frac{8}{27}$	$\frac{32}{27}$	$\frac{20}{27}$	$\hat{O}_{16}P_{36}$	$\frac{8}{27}$	$-\frac{4}{27}$	$\frac{20}{27}$
	$\hat{O}_{14}P_{36}$	$-\frac{4}{27}$	$\frac{2}{27}$	$\frac{35}{27}$				

Table 21. *Cont.*

$\sigma_i \cdot \sigma_j \, \lambda_i^c \cdot \lambda_j^c$	$\hat{O}_{12}$	$-\frac{8}{3}$	0	$-\frac{10}{3}$	$\hat{O}_{36}$	0	$-\frac{16}{9}$	$-\frac{20}{9}$
	$\hat{O}_{12}P_{36}$	$\frac{8}{27}$	$\frac{32}{27}$	$\frac{74}{27}$	$\hat{O}_{36}P_{36}$	$\frac{112}{27}$	$-\frac{8}{27}$	$\frac{88}{27}$
	$\hat{O}_{13}P_{36}$	$\frac{8}{27}$	$\frac{32}{27}$	$\frac{68}{27}$	$\hat{O}_{16}P_{36}$	$\frac{8}{27}$	$\frac{44}{27}$	$\frac{68}{27}$
	$\hat{O}_{14}P_{36}$	$\frac{4}{9}$	$\frac{14}{9}$	$\frac{7}{3}$				
$\sigma_i \cdot \sigma_j \sum_{a=1}^{3} \lambda_a(i)\lambda_a(j)$	$\hat{O}_{12}$	0	0	0	$\hat{O}_{36}$	0	0	0
	$\hat{O}_{12}P_{36}$	0	0	0	$\hat{O}_{36}P_{36}$	0	0	0
	$\hat{O}_{13}P_{36}$	0	0	0	$\hat{O}_{16}P_{36}$	0	0	0
	$\hat{O}_{14}P_{36}$	0	0	0				
$\sigma_i \cdot \sigma_j \sum_{a=4}^{7} \lambda_a(i)\lambda_a(j)$	$\hat{O}_{12}$	0	0	0	$\hat{O}_{36}$	0	0	0
	$\hat{O}_{12}P_{36}$	0	0	0	$\hat{O}_{36}P_{36}$	0	0	0
	$\hat{O}_{13}P_{36}$	0	0	0	$\hat{O}_{16}P_{36}$	0	0	0
	$\hat{O}_{14}P_{36}$	0	0	0				

By applying these sfc matrix elements for the $\Omega\Omega$ system, we dynamically solved the corresponding coupled-channel equation. The results are given in Table 22. We can see that no matter whether the calculations are single-channel or coupled-channel, this state would be deeply bound. It is noticed that due to the coupling from CC channel, the binding energy increases from 122.8 MeV to 129.7 MeV, and the RMS decreases from 0.66 fm to 0.65 fm, indicating that the coupling to the CC channel has some influence on forming this bound state.

Table 22. The same as Table 11 but for the $(\Omega\Omega)_{ST=00}$ state.

	$L = 0$	
	ΩΩ	**ΩΩ + CC**
E_b (MeV)	122.8	129.7
$\mathcal{R}$ (fm)	0.66	0.65

5. Conclusions

It is of importance to find a reasonable model to predict the possible dibaryon candidates. The chiral SU(3) quark model is just one of the most successful models, with which we can reasonably explain the experimental binding energies of baryon's ground state and deuteron, NN and YN scattering processes. By utilizing the same set of model parameters, we predicted the nonstrange d^* dibaryon with a binding energy of 84 MeV, which is consistent with the recent experimental data. We also found that the CC channel plays an important role in forming the bound d^* state.

Naturally, we would like to extend our study to some other interesting systems with different strangeness, due to the theoretical investigations of the CC channel on dibaryon candidates currently being scarce.

(1) In the single-channel calculation
According to the symmetry property, we firstly chose six interesting dibaryon candidates with different strangeness. They all belong to $\langle \mathcal{A}^{\rm sfc} \rangle \sim 2$. This kind of symmetry property will be most favorable in forming a bound structure, and thus, it is worth further performing the dynamical calculation. Then, we performed the dynamical investigation in the chiral SU(3) quark model by solving the resonating group method equation in the single-channel case. Indeed, the results indicate that all six dibaryon candidates become bound due to the symmetry property, and the interaction mechanism in scalar chiral fields, in particular, the sigma meson exchange, dominates the binding behavior.

(2) In the coupled-channel calculation
We extended it to include the CC channel. An easy and systematical method was utilized to work out the CC wave function for all six dibaryon candidates with different strangeness; then, all the sfc matrix elements were evaluated and nicely tabulated. By applying all these computed sfc matrix elements for different dibayon cases, we dynamically solved the corresponding coupled-channel equation for each case in the chiral SU(3)quark model. The calculated results are shown below.

(a) For the $S = 3$ case, we consider the coupling from the CC channel; thus, the configuration includes ($\Delta\Delta$+CC) or ($\Sigma^*\Delta$+CC), where there are tensor couplings from both OGE and pseudoscalar chiral field exchanges for each state. For $(\Delta\Delta)_{ST=30}$ and $(\Sigma^*\Delta)_{ST=3\frac{1}{2}}$ states, we found that both couplings, the CC coupling and tensor coupling, increment the binding energies by about 25 MeV and 20 MeV, respectively. The results clearly indicate that both states would become bound. The coupling to the CC channel plays an significant role in forming each state.

(b) Similarly, for the $S = 0$ case, the configuration includes ($\Delta\Delta$+CC), ($\Sigma^*\Delta$+CC), ($\Xi^*\Omega$+CC), or ($\Omega\Omega$+CC), in which there is no tensor coupling for each state. For $(\Delta\Delta)_{ST=03}$, $(\Sigma^*\Delta)_{ST=0\frac{5}{2}}$, $(\Xi^*\Omega)_{ST=0\frac{1}{2}}$, $(\Omega\Omega)_{ST=00}$ states with different strangeness (0, -1, -5 or -6), the calculated results show that the different CC channels increment by less than 10 MeV the corresponding binding energies. The CC channel has an obvious effect in the formation of each $S = 0$ dibaryon candidate.

Due to the theoretical investigations of the effect of the CC channel on each dibaryon candidate being currently scarce, we performed a systematical exploration on the possible and interesting dibaryon candidates with different strangeness. The obtained results are significant for helping us to acquire deeper understanding of the effect from the hidden color channel.

Here it should be mentioned that a quadratic potential for confinement was used in the calculations. Since the CC channel could be sensitive to the confinement potential, we would like to further investigate the linear potential for confinement in the future. Exploring in this direction will be of great interest and significant in helping us to profoundly understand QCD phenomenology.

Author Contributions: Conceptualization and methodology, L.D.; software, L.D.; validation, Y.W. and L.C.; formal analysis, T.Z.; data curation, Y.W. and L.C.; writing—original draft preparation, L.D.; writing—review and editing, L.D.; supervision, L.D.; project administration, L.D.; funding acquisition, L.D. All authors have read and agreed to the published version of the manuscript.

Funding: The project is supported by the National Natural Science Foundation of China under Grants No. 12175066 and 11975009.

Data Availability Statement: Data are contained within the article.

Conflicts of Interest: The authors declare no conflict of interest.

References

1. Adlarson, P.; Augustyniak, W.; Bardan, W.; Bashkanov, M.; Bergmann, F.S.; Berłowski, M.; Bhatt, H.; Büscher, M.; Calén, H.; Ciepał, I.; et al. [WASA-at-COSY]. Evidence for a New Resonance from Polarized Neutron-Proton Scattering. *Phys. Rev. Lett.* **2014**, *112*, 202301. [CrossRef]
2. Clement, H. On the History of Dibaryons and their Final Observation. *Prog. Part. Nucl. Phys.* **2017**, *93*, 195. [CrossRef]
3. Cho, S.; Hyodo, T.; Jido, D.; Ko, C.M.; Lee, S. H.; Maeda, S.; Miyahara, K.; Morita, K.; Nielsen, M.; Ohnishi, A.; et al. [ExHIC]. Exotic hadrons from heavy ion collisions. *Prog. Part. Nucl. Phys.* **2017**, *95*, 279. [CrossRef]
4. Dong, Y.B.; Huang, F.; Shen, P.N.; Zhang, Z.Y. Decay width of $d^*(2380) \to NN\pi\pi$ processes. *Phys. Rev. C* **2016**, *94*, 014003. [CrossRef]
5. Gal, A. The $d^*(2380)$ dibaryon resonance width and decay branching ratios. *Phys. Lett. B* **2017**, *769*, 436. [CrossRef]
6. Haidenbauer, J.; Petschauer, S.; Kaiser, N.; Meißner, U.G.; Weise, W. Scattering of decuplet baryons in chiral effective field theory. *Eur. Phys. J. C* **2017**, *77*, 760. [CrossRef]
7. Gongyo, S.; Sasaki, K.; Aoki, S.; Doi, T.; Hatsuda, T.;Ikeda, Y.; Inoue, T.; Iritani, T.; Ishii, N.; Miyamoto, T.; et al. [HAL QCD]. Most Strange Dibaryon from Lattice QCD. *Phys. Rev. Lett.* **2018**, *120*, 212001. [CrossRef]

8. Junnarkar, P.; Mathur, N. Deuteronlike Heavy Dibaryons from Lattice Quantum Chromodynamics. *Phys. Rev. Lett.* **2019**, *123*, 162003. [CrossRef]
9. Zhang, S.; Ma, Y.G. Ω-dibaryon production with hadron interaction potential from the lattice QCD in relativistic heavy-ion collisions. *Phys. Lett. B* **2020**, *811*, 135867. [CrossRef]
10. Dai, L.R.; Zhang, Y.N.; Sun, Y.L.; Shao, S.J. The nonstrange dibaryon and hidden-color effect in a chiral quark model. *Eur. Phys. J. A* **2016**, *52*, 295. [CrossRef]
11. Gongy, S.; Sasaki,K.; Miyamoto, T.; Aoki,S.; Doi, T.; Hatsuda,T.; Ikeda, Y. ; Inoue, T. Ishii,N. [HAL QCD]. $d^*(2380)$ dibaryon from lattice QCD. *Phys. Lett. B* **2020**, *811*, 135935. [CrossRef]
12. Morita, K.; Gongyo, S.; Hatsuda, T.; Hyodo, T.; Kamiya, Y.; Ohnishi, A. Probing ΩΩ and $p\Omega$ dibaryons with femtoscopic correlations in relativistic heavy-ion collisions. *Phys. Rev. C* **2020**, *101*, 015201.
13. Zhang, T.G.; Wang, Y.H.; Chen, L.N.; Dai, L.R. The effect of hidden-color channel on the structure of strangeness $S = -1$ dibaryon. *Mod. Phys. Lett. A* **2021**, *36*, 2150271. [CrossRef]
14. Clement, H.; Skorodko, T. Dibaryons: Molecular versus compact hexaquarks. *Chin. Phys. C* **2021**, *45*, 022001.
15. Zhang, T.G.; Dai, L.R.; Cai, X.J.; Chen, L.N.; Wang, Y.H. A study of hidden-color channel on the strangeness 1 dibaryon. *Eur. Phys. J. A* **2022**, *58*, 200. [CrossRef]
16. Urey, H.C.; Brickwedde, F.G.; Murphy, G.M. A Hydrogen Isotope of Mass 2. *Phys. Rev.* **1932**, *39*, 164. [CrossRef]
17. Gell-Mann, M. A schematic model of baryons and mesons. *Phys. Lett.* **1964**, *8*, 214. [CrossRef]
18. Jaffe, R.L. Perhaps a Stable Dihyperon. *Phys. Rev. Lett.* **1977**, *38*, 195. [CrossRef]
19. Dyson, F.L.; Xuong, N.H. $Y = 2$ states in SU(6) Theory. *Phys. Rev. Lett.* **1964**, *13*, 815. [CrossRef]
20. Mulders, P.J.G.; Aerts, A.T.M.; de Swart, J.J. Negative-Parity NN Resonances and Extraneous States. *Phys. Rev. Lett.* **1978**, *40*, 1543. [CrossRef]
21. Saito, K. Masses of the multi-quark states in the MIT bag model with the pion cloud. *Progr. Theoret. Phys.* **1984**, *72*, 674. [CrossRef]
22. Aerts, A.T.M.; Dover, C.B. On the production of the six-quark H dibaryon in the (K^-, K^+) reaction. *Phys. Rev. D* **1983**, *28*, 450. [CrossRef]
23. LaFrance, P.; Lomon, E.L. Six-quark resonance structures in nucleon-nucleon scattering. *Phys. Rev. D* **1986**, *34*, 1341. [CrossRef]
24. Oka, M.; Yazaki, K. Nuclear force in a quark model. *Phys. Lett. B* **1980**, *90*, 41. [CrossRef]
25. Maltman, K. On the possibility of deeply bound dibaryon resonances. *Nuc. Phys. A* **1985**, *438*, 669. [CrossRef]
26. Goldman, T.; Maltman, K.; Stephenson, G.J.; Schmidt, K. E.; Wang, F. Strangeness -3 dibaryons. *Phys. Rev. Lett.* **1987**, *59*, 627. [CrossRef]
27. Barnes, T.; Capstick, S.; Kovarik, M.D.; Swanson, E.S. NN core interactions and differential cross sections from one gluon exchange. *Phys. Rev. C* **1993**, *48*, 539. [CrossRef]
28. Li, Q.B.; Shen, P.N. Possible dibaryons with strangeness s=-5. *Phys. Rev. C* **2000**, *62*, 028202. [CrossRef]
29. Zhang, Z.Y.; Yu, Y.W.; Ching, C.R.; Ho, T.H.; Lu, Z.D. Suggesting a di-omega dibaryon search in heavy ion collision experiments. *Phys. Rev. C* **2000**, *61*, 065204. [CrossRef]
30. Dai, L.R.; Zhang, Z.Y.; Yu, Y.W. Structure of di-Ω dibaryon. *Chin. Phys. Lett.* **2006**, *23*, 3215.
31. Li, Q.B.; Shen, P.N.; Zhang, Z.Y.; Yu, Y.W. Dibaryon systems in chiral SU(3) quark model. *Nucl. Phys. A* **2001**, *683*, 487. [CrossRef]
32. Wang, F.; Ping, J.L.; Wu, G.H.; Teng, L.J.; Goldman, T. Quark delocalization, color screening, and dibaryons. *Phys. Rev. C* **1995**, *51*, 3411. [CrossRef]
33. Garcilazo, H.; Fernández, F.; Valcarce, A.; Mota, R.D. Bound states of ΔΔ and ΔΔΔ systems. *Phys. Rev. C* **1997**, *56*, 84. [CrossRef]
34. Gal, A.; Garcilazo, H. Three body calculation of the ΔΔ dibaryon candidate $\mathcal{D}_{03}(2370)$. *Phys. Rev. Lett.* **2013**, *111*, 172301. [CrossRef]
35. Bashkanov, M.; Brodsky, S.J.; Clement, H. Novel six-quark hidden-color dibaryon states in QCD. *Phys. Lett. B* **2013**, *727*, 438. [CrossRef]
36. Valcarce, A.; Garcilazo, H.; Mota, R.D.; Fernandez, F. Delta Delta and Delta Delta Delta bound states. *J. Phys. G* **2001**, *27*, L1. [CrossRef]
37. Valcarce, A.; Garcilazo, H.; Fernandez, F.; Gonzalez, P. Quark-model study of few-baryon systems. *Rept. Prog. Phys.* **2005**, *68*, 965. [CrossRef]
38. Yuan, X.Q.; Zhang, Z.Y.; Yu, Y.W.; Shen, P.N. ΔΔ dibaryon structure in chiral SU(3) quark model. *Phys. Rev. C* **1999**, *60*, 045203. [CrossRef]
39. Dai, L.R. ΔΔ dibaryon structure in extended chiral SU(3) quark model. *Chin. Phys. Lett.* **2005**, *22*, 2204.
40. Beiming, C.; Grönroos, J.; Ohlsson, T. Phenomenological mass model for exotic hadrons and predictions for masses of non-strange dibaryons as hexaquarks *Nucl. Phys. B* **2022**, *974*, 115616.
41. Chen, H.X.; Cui, E.L.; Chen, W.; Steele, T.G.; Zhu, S.L. QCD sum rule study of the $d^*(2380)$. *Phys. Rev. C* **2015**, *91*, 025204. [CrossRef]
42. Huang, H.X.; Ping, J.L.; Deng, C.R.; Wang, F. Theoretical study of a d^* resonance in the coupled ${}^3D_3$-${}^3G_3$ partial waves of nucleon-nucleon scattering. *Phys. Rev. C* **2014**, *90*, 064003. [CrossRef]
43. Dong, Y.B.; Shen, P.N.; Huang, F.; Zhang, Z.Y. Theoretical study of the $d^*(2380) \to d\pi\pi$ decay width. *Phys. Rev. C* **2015**, *91*, 064002. [CrossRef]

44. Huang, F.; Zhang, Z.Y.; Shen, P.N.; Wang, W.L. Is d* a candidate for a hexaquark-dominated exotic state?. *Chin. Phys. C* **2015**, *39*, 071001. [CrossRef]
45. Lü, Q.F.; Huang, F.; Dong, Y.B.; Shen, P.N.; Zhang, Z.Y. Six-quark structure of $d^*(2380)$ in a chiral constituent quark model. *Phys. Rev. D* **2017**, *96*, 014036. [CrossRef]
46. Dai, L.R.; Zhang, Z.Y.; Yu, Y.W.; Wang, P. *NN* interactions in the extended chiral SU(3) quark model. *Nucl. Phys. A* **2003**, *727*, 321. [CrossRef]
47. Zhang, Z.Y.; Yu, Y.W.; Shen, P.N.; Dai, L.R.; Faessler, A.; Straub, U. Hyperon-nucleon interactions in a chiral SU(3) quark model. *Nucl. Phys. A* **1997**, *625*, 59. [CrossRef]
48. Fernandez, F.; Valcarce, A.; Straub, U.; Faessler, A. The Nucleon-nucleon interaction in terms of quark degrees of freedom. *J. Phys. G* **1993**, *19*, 2013. [CrossRef]
49. Valcarce, A.; Fernandez, F.; Buchmann, A.; Faessler, A. Can one simultaneously describe the deuteron properties and the nucleon-nucleon phase shifts in the quark cluster model? *Phys. Rev. C* **1994**, *50*, 2246. [CrossRef]
50. Harvey, M. On the fractional parentage expansions of color singlet six quark states in a cluster model. *Nucl. Phys. A* **1981**, *352*, 301. [CrossRef]
51. Harvey, M. Effective nuclear forces in the quark model with Delta and hidden color channel coupling. *Nucl. Phys. A* **1981**, *352*, 326. [CrossRef]
52. Stancu, F. Group theory in subnuclear physics. *Oxford Stud. Nucl. Phys.* **1996**, *19*, 1.
53. An, C.S.; Riska, D.O.; Zou, B.S. Strangeness spin, magnetic moment, and strangeness configurations of the proton. *Phys. Rev. C* **2006**, *73*, 035207. [CrossRef]
54. Vijande, J.; Valcarce, A. Probabilities in nonorthogonal bases: Four-quark systems. *Phys. Rev. C* **2009**, *80*, 035204.
55. Yan, Y.; Srisuphaphon, S. Construction of multiquark states in group theory. *Prog. Part. Nucl. Phys.* **2012**, *67*, 496. [CrossRef]
56. Oka, M.; Yazaki, K. Short range part of baryon baryon interaction in a quark model. 1. Formulation. *Prog. Theor. Phys.* **1981**, *66*, 556.
57. Oka, M.; Yazaki, K. Short range part of baryon baryon interaction in a quark model. 2. Numerical Results for S-Wave. *Prog. Theor. Phys.* **1981**, *66*, 572.
58. Faessler, A.; Fernandez, F.; Lübeck, G.; Shimizu, K. The quark model and the nature of the repulsive core of the nucleon-nucleon interaction. *Phys. Lett. B* **1982**, *112*, 201.
59. Faessler, A.; Fernandez, F.; Lübeck, G.; Shimizu, K. The nucleon nucleon interaction and the role of the (42) orbital six quark symmetry. *Nucl. Phys. A* **1983**, *402*, 555. [CrossRef]
60. Zhang, Z.Y.; Brauer, K.; Faessler, A.; Shimizu, K. Influence of six quark bags on the NN interaction in a resonanting group scattering calculation. *Nucl. Phys. A* **1985**, *443*, 557. [CrossRef]
61. Yu, Y.W.; Zhang, Z.Y.; Shen, P.N.; Dai, L.R. Quark-quark potential from chiral symmetry. *Phys. Rev. C* **1995**, *52*, 3393. [CrossRef] [PubMed]
62. Straub, U.; Zhang, Z.; Bräuer, K.; Faessler, A.; Khadkikar, S.B.; Lübeck, G. Hyperon-nucleon interaction in the quark cluster model. *Nucl. Phys. A* **1988**, *483*, 686. [CrossRef]
63. Zhang, Z.Y.; Faessler, A.; Straub, U.; Glozman, L.Y. The baryon-baryon interaction in a modified quark model. *Nucl. Phys. A* **1994**, *578*, 573. [CrossRef]
64. Hill, D.L.; Wheeler, J.A. Nuclear Constitution and the Interpretation of Fission Phenomena. *Phys. Rev.* **1953**, *89*, 1102. [CrossRef]
65. Kamimura, M. Chapter V. A Coupled Channel Variational Method for Microscopic Study of Reactions between Complex Nuclei. *Suppl. Prog. Theor. Phys.* **1977**, *62*, 236. [CrossRef]
66. Dai, L.R. The mixing of scalar mesons and the baryon-baryon interaction. *Eur. Phys. J. A* **2011**, *47*, 26. [CrossRef]
67. Kusainov, A.M.; Neudatchin, V.G.; Obukhovsky, I.T. Projection of the six-quark wave function onto the *NN* channel and the problem of the repulsive core in the *NN* interaction. *Phys. Rev. C* **1991**, *44*, 2343. [CrossRef]
68. Buchmann, A.; Fernandez, E.; Yazaki, K. Gluon and pion exchange currents in the nucleon. *Phys. Lett. B* **1991**, *269*, 35. [CrossRef]
69. Henley, E.M.; Miller, G.A. Excess of d over u in the proton sea quark distribution. *Phys. Lett. B* **1990**, *251*, 453. [CrossRef]
70. Zhang, D.; Huang, F.; Dai, L.R.; Yu, Y.W.; Zhang, Z.Y. Study of $N\bar{\Omega}$ systems in a chiral quark model. *Phys. Rev. C* **2007**, *75*, 024001. [CrossRef]
71. Dumbrajs, O.; Koch, R.; Pilkuhn, H.; Oades, G. c.;Behrens, H.; De Swart, J. j.; Kroll, P. Compilation of Coupling Constants and Low-Energy Parameters. 1982 Edition. *Nucl. Phys. B* **1983**, *216*, 277. [CrossRef]
72. Arndt, R.A.; Strukovsky, I.I.; Workman, R.L. Updated analysis of *NN* elastic scattering data to 1.6 GeV. *Phys. Rev. C* **1994**, *50*, 2731. [CrossRef] [PubMed]
73. Dai, L.R.; Su, H.; Li, B.; Shao, S.J.; Sun, Y.L. Dibaryons without strangeness. *Nucl. Phys. Rev.* **2017**, *34*, 035.